Simulating Water and Pollutant Transport in Bark, Charcoal and Sand Filters for Greywater Treatment

Susanna Ciuk Karlsson

Faculty of Natural Resources and Agricultural Sciences
Department of Energy and Technology
Uppsala

Report (Department of Energy and Technology)
Licentiate thesis/Report 085
ISSN 1654-9406
ISBN (print version) 978-91-576-9324-2
ISBN (electronic version) 978-91-576-9325-9

Print: SLU Service/Repro, Uppsala 2015

Simulating Water and Pollutant Transport in Bark, Charcoal and Sand Filters for Greywater Treatment

Abstract

A septic tank combined with a sand filter is the most common onsite wastewater treatment system worldwide, since it is a simple, lowcost and reliable treatment method. Alternatives to sand in filters could be advantageous in terms of availability of material and enhanced treatment properties.

In this study, flow dynamics and pollutant transport in three filter materials; sand, pine bark and activated charcoal, intermittently dosed with artificial greywater, were simulated using the HYDRUS wetland module. The simulated results were compared with observations from laboratory filters and model hydraulic and microbial parameters were calibrated. Emphasis was placed on simulating the removal of organic pollutants by each filter type. Furthermore, for the bark and charcoal filters, removal of organic matter was simulated for different hydraulic and organic loading rates (HLR = 32 and 64 l m^{-2} day^{-1} and OLR = 13-6 and 28 g BOD_5 m^{-2} day^{-1}).

Comparing simulated with measured cumulated effluent volume, the normalised root mean square error for all three filter materials was small (0.7-3.5%). The simulated bark filter COD removal in different loading regimes (HLR = 32 and 64 l m^{-2} day^{-1}, OLR = 13-16 and 28 g BOD_5 m^{-2} day^{-1}) was overestimated by 13-20 percentage points compared with the measured values. When release of organic matter from the bark material itself was accounted for, the difference was reduced to 2-10 percentage points. Simulation of the charcoal filter demonstrated 94 and 91 % removal of COD for HLR = 32 and OLR = 13 - 16 g BOD_5 m^{-2} day^{-1}, which compared well with the measured values, 95 ± 2 % and 89 ± 11 %, respectively. However, simulated COD removal for Run 2 (70%) and Run 5 (72%) was low compared with the measured values (90 ± 7 and 84 ± 4 %). The measured sand filter effluent concentration of COD was 245 mg l^{-1} and the simulated effluent concentration of COD was 134 mg l^{-1} for HLR = 32 and OLR = 14 g BOD_5 m^{-2} day^{-1}. After including an effect of water flow along the column wall in the model, the simulated effluent concentration of COD was 337 mg l^{-1}.

These simulations of bark, charcoal and sand filters improved understanding of filter functions and identified possible filter design developments.

Keywords: activated charcoal, greywater, HYDRUS wetland module, organic matter removal, pine bark, sand, simulation, vertical flow filter

Author's address: Susanna Ciuk Karlsson, SLU, Department of Energy and Technology
PO Box 7032, SE-750 07 Uppsala, Sweden
E-mail: susanna.ciuk.karlsson@slu.se

Dedication

To Tomas, *you're my Shangri La*.

You only have power over people so long as you don't take everything away from them. But when you've robbed a man of everything he's no longer in your power — he's free again.

Aleksandr Solzhenitsyn

Contents

List of Publications

This thesis is based on the work contained in the following papers, referred to by Roman numerals in the text:

I Susanna Ciuk Karlsson, Langergraber, G., Pell, M., Dalahmeh, S., Vinnerås, B., Jönsson H. (2015). Simulation and verification of hydraulic properties and organic matter degradation in sand filters for greywater treatment. *Water Science and Technology* 71, 426-433.

II Susanna Ciuk Karlsson, Langergraber, G., Pell, M., Dalahmeh, S., Jönsson, H. (2015). Simulation of water flow and organic matter removal in bark and charcoal filters for greywater treatment (Manuscript). *Submitted.*

Paper I is reproduced with the permission of the publisher.

The contribution of Susanna Ciuk Karlsson to the papers included in this thesis was as follows:

I Participated in planning the work and conducted the computer modelling. Interpreted the simulated data together with the co-authors. Had the main responsibility for writing the manuscript and producing the diagrams and tables.

II Participated in planning the work and conducted the computer modelling. Interpreted the simulated data together with the co-authors. Had the main responsibility for writing the manuscript and producing the diagrams and tables.

1 Introduction

Water scarcity, defined as annual water supply below 1000 m^3 water per person, affects 700 million people in 43 countries today (WWAP, 2012). Generally, this means that water demand by all sectors (agricultural, industrial and urban) cannot be satisfied. Furthermore, it is predicted by that by 2015, 1.8 billion people will be living with absolute water scarcity, an even worse condition defined as annual water supply below 500 m^3 water per person.

Reuse of greywater (*i.e*. household wastewater, excluding wastewater from toilets) can help sustain natural water resources (Nolde, 1999). Pit latrines are used worldwide by an estimated 1.77 billion people (Graham & Polizzotto 2013). The wastewater from this type of household is either source separated by default, as greywater is not released into the pit latrine, or may easily be kept separate from the pit latrine. Appropriate treatment of greywater can enable sustainable reuse of large quantities of water and prevent release of pollutants to natural water bodies.

Furthermore, 54% of the world's population lives in urban areas, with the projection that this number will increase to 66% by 2050 (UN, 2014). Between 15 and 20 % of the food consumed globally is produced by urban agriculture (Corbould, 2013). Implementing small-scale treatment of greywater in urban agriculture for re-use of water for irrigation could improve crop yields and also protect the environment from release of untreated greywater and/or overuse of natural water bodies. The suitability of using correctly treated greywater for irrigation is supported by WHO (2006).

Regarding general water usage, approximately 70% is used for irrigation in agriculture, 20% for industrial use and 10% for direct human use (drinking, washing *etc*.). Urban wastewater is a significant point source of pollutants (WWAP, 2012). Conveying wastewater to a central wastewater treatment plant is common procedure in industrialised, high-income countries. However, centralised wastewater treatment systems require complex infrastructure,

expert knowledge and high investments. An alternative to centralised wastewater treatment is small-scale and/or onsite treatment. A septic tank combined with a sand filter is one of the most common onsite wastewater treatment systems worldwide, since it is a simple, low-cost and reliable treatment solution (USEPA 2002). The sand filter treats influent water through physical filtration, chemical transformation and biological processes in the biofilm developed by microbial growth as a response to the nutrients present. Common designs of sand filter systems are trenches and mounds.

Using filter media other than sand could make filter and infiltration systems more accessible and enhance removal of pollutants. Bark is frequently available as a cheap waste product from industry and charcoal can be produced from lignocellulosic waste material. Seki *et al.* (1997) compared milled coniferous bark with activated carbon in terms of removal of heavy metals from water and concluded that bark could be used for pollution removal systems. Argun *et al.* (2009) also concluded that pine bark is an effective adsorbent of the heavy metals cadmium, lead, copper and nickel and that bark could therefore be a good alternative to more costly materials such as activated carbon. Lens *et al.* (1994) used laboratory columns to determine the treatment capacity of peat, bark and woodchips as filter materials for treating primary domestic sewage by percolation. Lens *et al.* (1994) concluded that bark and peat were applicable materials, whereas woodchips had insufficiently high capacity (26%) to lower the chemical oxygen demand (COD).

Scholz & Xu (2002) investigated the treatment efficiency of vertical flow filters containing different macrophytes and granular media with different adsorption capacities. They used six filters with different layering of nine separate sand and charcoal filter materials (cobblestones, coarse gravel, fine gravel, pea-gravel, coarse sand, medium sand, Filtralite, granular activated carbon and charcoal). The filters were fed for 10 months with river water polluted by drainage water and sewage, and with copper and lead also added in the experiment. It was found that addition of expensive adsorption filter materials did not cause a statistically significant increase in removal of copper and lead. Furthermore, the overall filtration performance in terms of biochemical oxygen demand (BOD_5) and turbidity removal was similar for all filters during the 10 months of operation. However, Dalahmeh *et al.* (2012) found that greywater treatment with bark or charcoal as filter materials outperformed sand as the filter medium.

More research is needed to determine the full capacity of bark and charcoal as alternative filter materials to sand. Moreover, almost all available design guidelines for sand filters are based on empirical rules-of-thumb or simple first-order decay models (Langergraber *et al.*, 2009). Modelling flow and

compound transport can provide a practical tool for design and operation optimisation of filter systems. Common models for such purposes include PHREEQC (Parkhurst & Appelo, 2013), PHWAT (Mao *et al.*, 2006), FITOVERT (Giraldi *et al.*, 2010) and the HYDRUS wetland module (Langergraber & Šimůnek, 2012).

PHREEQC (Parkhurst & Appelo, 2013) is a computer programme written in C and C++ and performs a wide variety of aqueous geochemical calculations. PHREEQC is suitable for speciation and saturation-index calculations, batch-reaction and one-dimensional (1D) transport calculations with reversible and irreversible reactions, surface complexation, ion exchange equilibria, specified mole transfers of reactants, kinetically controlled reactions and mixing of solutions, and also considers pressure and temperature changes. Furthermore, PHREEQC provides an inverse modelling tool for finding sets of mineral and gas mole transfers that account for differences in composition between waters. Herrmann *et al.* (2013) successfully used PHREEQC to simulate the removal of phosphate in laboratory-scale filter columns for domestic wastewater treatment using calcium-silicate sorbent (Filtralite) as the filter medium.

Mao *et al.* (2006) combined PHREEQC with a density-dependent groundwater flow and solute transport model (SEAWAT; Guo & Langevin, 2002) for simulating multi-component reactive transport in variable density groundwater flow and named the combined model PHWAT. The modular design of PHWAT allows easy incorporation of individual submodules. PHWAT was coupled with a modular numerical model describing biomass growth by Brovelli *et al.* (2009) to simulate clogging by microbial biomass of porous media, using experimental data from a sand filter fed with a solution containing growth medium.

HYDRUS is Microsoft Windows-based software for modelling two- and three-dimensional movement of water, solutes and heat in variably saturated porous media (Šimůnek *et al.*, 2011). HYDRUS can be coupled with the HYDRUS wetland module, which considers transport and reactions in soil, including typical pollutants of wastewater such as organic matter, nitrogen and phosphorus (Langergraber & Šimůnek, 2012). The HYDRUS wetland module was used by Rizzo *et al.* (2014) to simulate the response of a laboratory horizontal flow constructed wetland to variable loads of synthetic sewage wastewater. They found that the overall removal efficiency of simulated COD effluent was similar to experimental observations.

This is only a small selection of the ongoing work on hydrological and geochemical modelling. However, to the best of my knowledge the HYDRUS

wetland module or similar software has not been used previously for modelling vertical flow bark, charcoal and sand filters subjected to greywater.

All models mentioned above are based on the same or similar mathematical equations for flow and solute transport, but a unique feature of the HYDRUS wetland module is the specialisation on constructed wetlands for wastewater treatment. In particular, it deals with the unsaturated flow occurring in vertical flow filters by applying differential flow equations, as opposed to rudimentary equations governing plug flow.

1.1 Objectives

The overall aim of this licentiate project was to test whether the flow and treatment processes of greywater in vertical bark, charcoal and sand filters with unsaturated flow could be accurately simulated using computer modelling.

Specific objectives were to: (1) identify and evaluate procedures to increase the fit of the sand filter flow simulated results compared with observations (**Paper I**); (2) include and calibrate biomass in the filter media as a main treatment mechanism (**Paper I** and **Paper II**); (3) simulate organic matter degradation in vertical flow bark, charcoal and sand filters (**Paper I** and **Paper II**); and (4) simulate water flow and organic matter degradation under different hydraulic and organic loading rates for bark and charcoal filters (**Paper II**).

To achieve these objectives, the software HYDRUS with its add-on wetland module was chosen as the modelling tool. The work was focused on calibrating the model parameters and evaluating the models by comparing simulated results with previous measurements obtained in a laboratory-scale set-up testing sand, bark and charcoal filters.

1.2 Structure of the work

Paper I in this thesis focused on modelling the performance of a vertical flow sand filter subjected to greywater. A novel feature of that study was varying the number of calibrated flow model parameters, which contributed to a better understanding of the model dynamics (Figure 1). The performance of vertical flow bark and charcoal filters subjected to greywater was studied in **Paper II**. A novel feature of that study was the simulation of organic matter removal by bark and charcoal filters under four loading regimes with different combinations of hydraulic loading rates (HLR; 32 or 64 l m^{-2} day^{-1}) and organic loading rates (OLR; 13-16 or 28 g BOD_5 m^{-2} day^{-1}).

Calibrations of hydraulic parameters, biomass growth and simulation of filter effluent organic matter concentrations during a fixed artificial greywater loading regime were performed in both **Paper I** and **Paper II** (Figure 1).

The results obtained in **Papers I** and **II** are compared and discussed in this thesis essay in relation to the stated objectives. In addition, a detailed sensitivity analysis of the HYDRUS wetland module and preliminary results for simulation of nitrogen and phosphorus compounds is reported in this essay, followed by suggestions for future research.

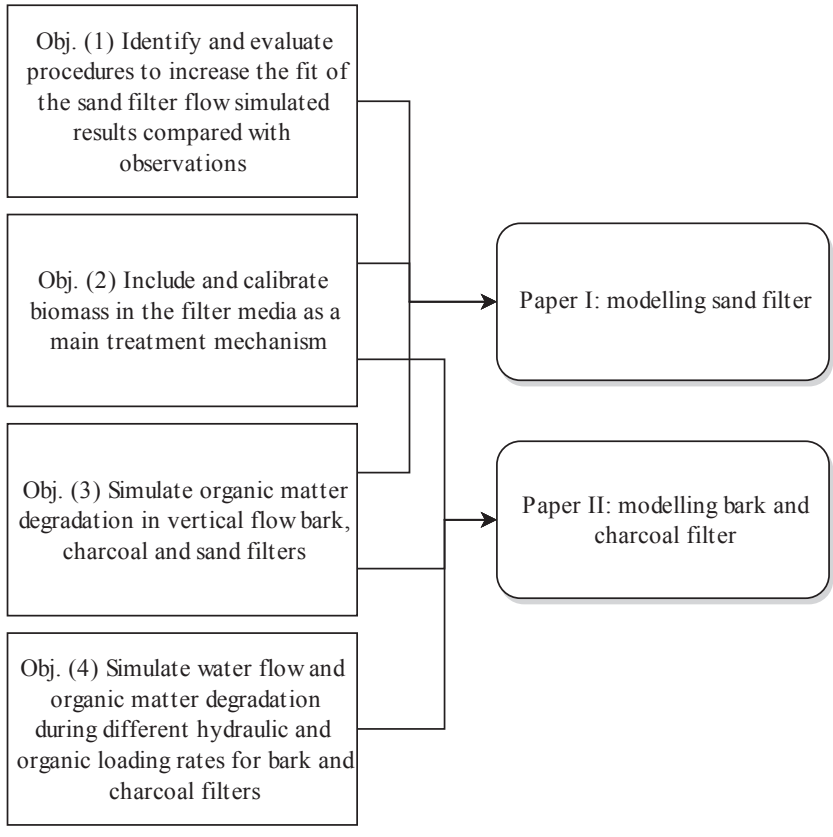

Figure 1. Objectives of the studies reported in **Paper I** and **Paper II.**

2 Background

2.1 Wastewater treatment by infiltration

The composition of household wastewater varies greatly depending on circumstances such as water availability and lifestyle of household members (*e.g*. presence of small children, animals, chemical use). In general, greywater contains lower levels of organic matter and nutrients than mixed household wastewater, since urine, faeces and toilet paper are not included (Eriksson *et al.*, 2002).

Greywater may contain pathogens, mainly originating from faecal contamination (*e.g*. from washing diapers), skin and mucous tissue and/or food handling (Maimon *et al.*, 2010). Due to use of household chemicals such as detergents, soaps and beauty products *etc*., greywater also contains xenobiotic micro-pollutants that are harmful for the environment (Donner *et al.*, 2010). Due to food waste from kitchens in particular, greywater also contains organic matter. Organic matter is commonly measured as biological oxygen demand (BOD) or chemical oxygen demand (COD). If wastewater containing organic matter reaches a natural water body, the organic matter is degraded there, creating a risk of depleting the oxygen, causing anaerobic conditions and sulphide production (Eriksson *et al.*, 2002).

The most commonly used systems for onsite treatment and release of wastewater are subsurface wastewater infiltration systems (Subramani & Akela, 2014). The wastewater is first directed to a septic tank, which acts as a combined settling tank and anaerobic bioreactor that removes most of the solid organic matter and, depending on the conditions (*e.g*. temperature), also digests some dissolved organic matter and may mineralise nitrogen (*i.e*. organic nitrogen is transformed to ammonium). The septic tank effluent is rich in organic matter and nutrients and may contain human pathogens. The effluent is infiltrated through permeable, unsaturated natural soil, which is the definition

of infiltration. If suitable soil is unavailable, a fill material can be used instead. As the wastewater passes through the soil or fill material, it is subjected to physical, chemical and biochemical processes and reactions, leading to removal of pollutants. The infiltration zone functions in an equivalent way to a fixed-film bioreactor. Organic pollutants in the wastewater are degraded by microorganisms, a process which requires oxygen. If the available oxygen is not sufficient, the metabolic processes of the microorganisms are retarded and over time the microbial community will adapt and change to anaerobic processes (Subramani & Akela, 2014).

The top of the infiltration zone is the most biologically active and is also where most sorption reactions occur, because the negative water potential in the unsaturated zone causes percolating water to move into the micropores of the infiltration material, which increases the contact surface (Subramani & Akela, 2014).

In an infiltration system, when the wastewater reaches the bottom of the infiltration material, it continues to percolate through the underlying soil and finally to the groundwater (Subramani & Akela, 2014). Another alternative, more common for filter systems, is to have a non-permeable layer in the bottom of the infiltration material and direct the effluent water through a pipe for release to either a ditch or directly into a nearby water body.

2.2 Microbiology

The potential of subsurface infiltration systems to remove pollutants from wastewater by microbial action has led to the concept of "living filters" (Kristiansen, 1981). The microflora in sand filters loaded with septic tank effluent consists of numerous different viruses, bacteria, fungi, protozoa and metazoa (Kristiansen, 1981; Calaway, 1957).

Microbial activity within filters and infiltration systems can be considered to be closely related to soil microbiology. Microorganisms make up 0.5% of soil mass, even though the typical prokaryote microbial cell is only about 0.5 μm (Tate, 1995). There are more than 10^{16} microorganisms in a ton of soil (compared with 10^{11} stars in our galaxy). This led Curtis and Sloan (2005) to describe studying microbial diversity as exploring a largely unknown microbial universe, comparable with exploring outer space. Furthermore, the biochemical potential of soil microbes is significantly greater than that expressed at any particular point in time, as the populations are a mixture of actively growing and resting cells (Tate, 1995). Microbial growth in soil occurs at microsites, as a result of the spatial and temporal non-homogeneity of energy supply. In

addition, bacteria prefer in particular to attach to surfaces where phase transitions are occurring (Tate, 1995).

A soil site needs to be evaluated both at the macro and micro scale to properly assess the conditions for microbial growth (Tate, 1995). Soil site properties which interact with microorganisms are nutrient and energy availability, moisture, oxygen availability, surface charges, redox potential, pH and temperature. Carbon resources generally control the microbial population, but as microbes are totally dependent on water for their activities, moisture is also essential. There is rarely only one stress factor limiting microbial growth and it is most often difficult to determine the exact conditions at each microsite (Tate, 1995).

Microorganisms mainly consist of organic carbon, nitrogen and phosphorus. Aside from being an energy source, organic carbon is the building material for the microbial skeleton. Nitrogen is needed by the microorganisms to form proteins, cell wall components and nucleic acids. Phosphorus is a key substrate in the energy generation system and is also needed to form nucleic acids and phospholipids. For microorganisms to reach their full potential in wastewater treatment systems, a correct ratio of C:N:P in the substratum is vital (Thompson *et al*., 2005). Droste (1997) gives a general chemical formula for microbial biomass of $C_5H_7O_2NP_{0\text{-}074}$ which corresponds to a C:N:P ratio of 100:5:1.

Unlike soil, infiltration and filter-type systems for treatment of wastewater provide conditions with continuous inflow of energy, carbon and nutrients for the microbes to thrive on. Wastewater from particular households is likely to be homogeneous over time compared with the natural energy inputs to soils and the microflora within an infiltration system will therefore be highly specialised.

According to Calaway (1957), while filtration and adsorption play an important part in the purification of wastewater in intermittent sand filters, biological oxidation is the most important function.

2.3 Computer modelling

The first device to be used for mathematical calculations in human history was arguably the tally stick. Tally sticks are used to record and document numbers, quantities and even messages, mostly for financial transactions. The first tally stick ever used by Man is believed to be the Ishango bone, dated to the Upper Paleolithic era (50 000-10 000 years ago) (Rudman, 2006). However, the most rapid progress in the field of computer modelling and simulations has been over the last two decades.

Computer simulations are tools for extending the class of tractable mathematics, which thereby support scientific progress (Frigg & Reiss, 2007). However, computer modelling methods are argued by some to be essentially different from the understanding and evaluation of traditional theories (Humphreys, 2004) and are thought of as an intermediate between traditional theoretical science and its empirical methods of experimentation and observation (Rohrlich, 1990).

In contrast, Frigg & Reiss (2007) argue that simulation is not different from the empirical methods of experimentation and observation. They claim that like computer modelling, many physical experiments could be perceived as creating a parallel world where explanations are found for some real world phenomena, in the sense that experiments are conducted on proximate systems rather than the target system themselves.

However, Peschard (2010), argues that there is a misconception in the assumption that experimentation and simulation are similar, in the sense that what is manipulated is a system representing a target system. The confusion lies with the intermixing of the *epistemic target* and *epistemic motivation* of an experiment. To gain knowledge (epistemic motivation) on some non-computer related real-life phenomenon, computer modelling can be used. However, the computer (the epistemic target) is only similar to the studied phenomenon in very abstract terms.

How well a computer model can represent reality brings in the processes of *verification* and *validation*. A common interpretation of the term verification is that the computer simulation has been tested for algorithm inconsistencies within the code and that numerical errors such as round-off errors, propagating errors in iterative methods and errors in discretisation have been evaluated (Oberkampf & Roy, 2010). Validation, in contrast to verification, is commonly meant as evaluating how well the simulation represents reality. The most common way of doing this is to compare simulated results with observed data (Oberkampf & Roy, 2010).

However, the concepts of verification and validation of computer models can be questioned. For example, Oreskes *et al.* (1994) argue that verification is only possible in closed systems and, since numerical models of natural systems are open, verification/validation is unattainable. Furthermore, in 'verification' of numerical solutions, they argue that the congruence between a numerical and an analytical solution indicates nothing about the agreement of either one with material reality.

Oreskes *et al.* (1994) point out another important issue, namely that if the verification/validation fails, the fault can be either in the hypothesis or in the auxiliary assumptions. Even when the model is validated in the sense that

simulated data match observed data, more than one set of parameters chosen for the model can produce the same output, a situation which is referred to as non-uniqueness or underdetermination. In the case of non-uniqueness, it can be difficult to judge which of the parameter sets is more correct.

Regardless of the debate on the nature of computer modelling and whether it can truly represent reality, the impact of computer simulations on modern science can be found almost everywhere. According to Rohrlich (1990), computer simulations can be seen as a milestone similar to those reached by Galileo (start of the empirical approach) and Newton and Laplace (start of the deterministic mathematical approach to dynamics).

2.4 HYDRUS wetland module

The software HYDRUS with its add-on wetland module was chosen as the modelling tool used for both **Paper I** and **Paper II**, mainly because of its specialisation in relevant compounds found in household wastewater and its ability to manage unsaturated flow simulation.

HYDRUS is a Microsoft Windows based software for modelling two- and three-dimensional movement of water, solutes and heat in variably saturated porous media (Šimůnek *et al.*, 2011). HYDRUS uses partial differential equations; a modified form of Richard's equation for water flow and convection-dispersion type equations for heat and solute transport (Šimůnek *et al.*, 2011):

$$\frac{\partial \theta}{\partial t} = \frac{\partial}{\partial x_i}\left[K\left(K_{ij}^{A}\frac{\partial h}{\partial x_j} + K_{iz}^{A}\right)\right] - S \qquad (1)$$

where θ is volumetric water content ($cm^3\ cm^{-3}$), h is pressure head (cm), S is a sink term (h^{-1}), x_i is spatial coordinates (cm), t is time (h^{-1}), K_{ij}^{A} is a component of a dimensionless anisotropy tensor $\boldsymbol{K}^{A}$ and K is an unsaturated hydraulic conductivity function, (cm h^{-1}). The unsaturated hydraulic conductivity function in the modified Richard's equation is the product of the relative hydraulic conductivity (K_r, cm h^{-1}) and the saturated hydraulic conductivity (K_s, cm h^{-1}):

$$K(h,x,y,z) = K_s(x,y,z)K_r(h,x,y,z) \qquad (2)$$

HYDRUS provides five different analytical models for the hydraulic parameters of the unsaturated hydraulic conductivity function: the equations by Brooks and Corey (1964), the modified van Genuchten type equations by Vogel and Cislerová (1988), the lognormal distribution model of Kosugi

(1995), the dual porosity model by Durner (1994) and the van Genuchten–Mualem model (van Genuchten, 1980).

The van Genuchten- Mualem model is that most commonly used and was chosen for the modelling in **Papers I** and **II**. It gives the water content as:

$$\theta(h) = \begin{cases} \theta_r + \frac{\theta_s - \theta_r}{[1+|\alpha h|^n]^m} & h < 0 \\ \theta_s & h \geq 0 \end{cases} \quad (3)$$

Furthermore, the hydraulic conductivity is given by:

$$K(h) = K_s S_e^l \left[1 - \left(1 - S_e^{1/m}\right)^m\right]^2 \quad (4)$$

where θ_r and θ_s are the residual and saturated water content ($cm^3\ cm^{-3}$), α is the inverse of the air entry value (cm^{-1}), n is the pore-size distribution index (-) and l is the pore-connectivity parameter (-). In this thesis, the saturated water content was taken to be the porosity. Furthermore, m is given by:

$$m = 1 - \frac{1}{n} \qquad n > 1 \quad (5)$$

For the macroscopic transport of components in the system, the following equation is used:

$$\frac{\partial \theta c_i}{\partial t} + \frac{\partial \rho S_i}{\partial t} = \nabla(\theta \boldsymbol{D}_i \nabla c_i) - \nabla(\boldsymbol{q} \nabla c_i) + S c_{s,i} + r_i \quad (6)$$

where i = 1,…, N (N is number of components), c_i is the concentration in the aqueous phase ($mg\ cm^{-3}$), S_i is the concentration in the solid phase ($mg\ mg^{-1}$), θ is the volumetric water content ($cm^3\ cm^{-3}$), ρ is the soil bulk density ($mg\ cm^{-3}$), D_i is the effective dispersion tensor (cm^2) to include molecular diffusion and longitudinal and transverse dispersion, q is the volumetric flux density ($cm^3\ cm^{-2}\ h^{-1}$), S is a source-sink term ($cm^3\ cm^{-3}\ h^{-1}$), $c_{s,i}$ is the concentration of the source or sink ($mg\ cm^{-3}$) and r_i is a reaction term ($mg\ cm^{-3}\ h^{-1}$).

The partial differential equations in HYDRUS are numerically solved using the finite element method. The finite element works analogously to the idea that a circle can be constructed using numerous tiny, connected straight lines. In the finite element method, numerous simple element equations over small subdomains (finite elements) approximate a more complex equation over the complete domain. The finite element subdomain differs depending on the dimension of the problem. For 1-D, the subdomain is a line with one node located at each end. For 2-D, the element is a triangle with one node in each

corner of the triangle and for 3-D the element is a tetrahedron with one node in each corner. The field variables, *i.e.* the dependent variables of interest governed by the differential equations, are explicitly calculated in the nodes at each time step. The values at the nodes are then used to approximate the values in the element interior by interpolation (Polyanin, 2002).

The HYDRUS wetland module considers transport and reactions in soil, including typical pollutants of wastewater such as organic matter, nitrogen and phosphorus (Langergraber & Šimůnek, 2012). The module is based on the principles of the Activated Sludge Model (ASM) (Henze *et al.*, 1987). ASM is the collective name for several mathematical methods that model activated sludge systems and is often applied to full-scale wastewater treatment plants. Activated sludge systems depend on treating wastewater using air and biological flocs composed of bacteria and protozoa.

The HYDRUS wetland module has two settings; Constructed Wetland Model No. 1 (CWM1) and Constructed Wetlands 2D (CW2D). CWM1 applies to horizontal flow filter types with saturated flow, while CW2D simulates unsaturated flow in *e.g.* vertical flow filter types (Langergraber & Šimůnek, 2012). CW2D has 12 components:

- Dissolved oxygen (*SO*, mg l^{-1})
- Readily biodegradable organic matter (*CR*, mg COD l^{-1})
- Slowly biodegradable organic matter (*CS*, mg COD l^{-1})
- Inert organic matter (*CI*, mg COD l^{-1})
- Heterotrophic microorganisms (*XH*, µg COD g filter material^{-1})
- Nitrosomonas, autotrophic bacteria (*NS*, µg COD g filter material^{-1})
- Nitrobacter, autotrophic bacteria (*NB*, µg COD g filter material^{-1})
- Ammonium nitrogen, NH^{+}_{4}-N and ammonia nitrogen, NH_3-N (*NH4N*, mg l^{-1})
- Nitrite nitrogen, NO_2-N (*NO2N*, mg l^{-1})
- Nitrate nitrogen, NO_3-N (*NO3N*, mg l^{-1})
- Dinitrogen gas, N_2 (*N2*, mg l^{-1})
- Inorganic phosphorus, PO_4^{3-} (*IP*, mg l^{-1})

Key processes included in CW2D are hydrolysis (conversion between the organic matter fractions *CS*, *CR* and *CI*) and microbial growth and lysis for *XH*, *NS* and *NB* (Langergraber & Šimůnek, 2012). The full equations of HYDRUS CW2D can be found in Appendix A.

3 Material and methods

The input data used for modelling in this thesis were taken from a series of previous studies testing the performance of vertical flow bark, charcoal and sand filters treating greywater in laboratory-scale filter experiments (Dalahmeh *et al.*, 2012, 2014a, 2014b). Supplementary data on cumulative effluent volume were obtained from another experiment (Karlsson, 2012). A brief description of the experiments is presented in the following sections.

3.1 Experimental set-up

The same laboratory-scale experimental set-up was used in all experiments form which data were obtained for this thesis. The set-up consisted of acrylic columns (20 cm diameter) filled with filter material to a height of 60 cm (Figure 2). There were six columns in total (two replicate filters each of bark, charcoal and sand). The filter materials were sieved so that the effective particle size and uniformity coefficient were equal for all three filter types. Other characteristics of the filter material, such as porosity and saturated hydraulic conductivity, were measured.

The filter system was designed for intermittent feeding, with three portions (70, 10 and 20 %) of the total daily load applied at 09.00, 16.00 and 20.00 h, respectively. The intermittent artificial greywater loadings to which the filters were subjected contained only a small amount of solid particles (100-120 mg l^{-1}), in order to mimic greywater that had already passed through a septic tank or other pre-treatment step. The feeding procedure for the filters was computer-controlled, with a pumping system connected to a heater to keep a constant temperature of 25 ^{o}C, which corresponded to room temperature. The loads were evenly distributed through sprinklers. During the experiments the influent and effluent from the filters were collected and analysed for pollutant concentrations (*e.g.* organic matter, nitrogen and phosphorus compounds).

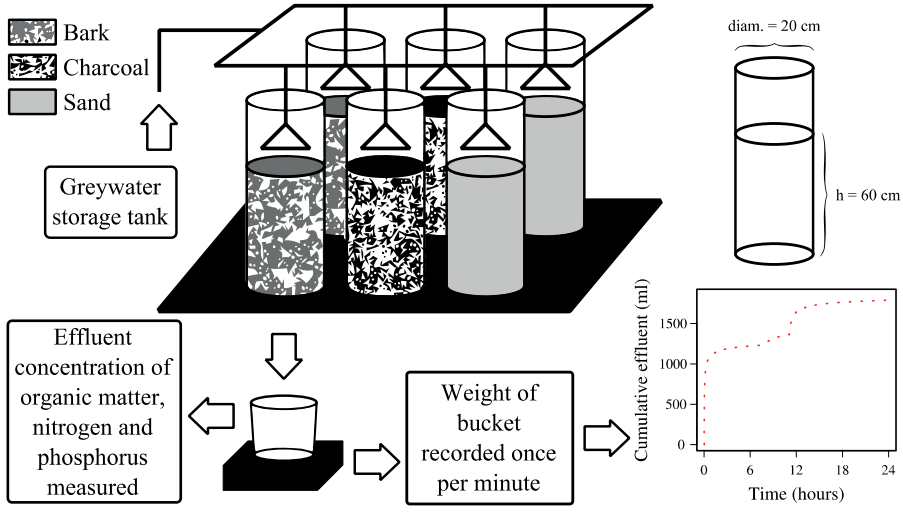

Figure 2. Experimental set-up of the bark, charcoal and sand vertical flow filters from which input data were obtained for the modelling work presented in this thesis.

3.1.1 Fixed hydraulic and organic loading regime

For the first experiment (Run 0), the filters were fed 1 l artificial greywater per day, which is equal to a hydraulic loading rate (HLR) of 32 l m^{-2} day^{-1} (Figure 3). The artificial greywater was prepared in the laboratory by mixing various ingredients such as shampoo, washing power and maize oil to obtain a fluid similar to real household greywater, although omitting solid waste. The artificial greywater was prepared according to a strict recipe to ensure consistent composition throughout the experiment. It was inoculated with a small volume of wastewater from a municipal wastewater treatment plant to get a natural microflora and was dosed at an OLR of 14 g BOD_5 m^{-2} day^{-1}.

To assess the microbial activity in the filter materials, substrate-induced potential respiration was measured at different depths (0-2, 20, 40 and 60 cm) in the filters on day 14, 28, 42, 56 and 84 of the 112-day run period (Figure 3).

Measured influent and effluent concentrations of nitrogen, phosphorus and organic matter in the filters were used in the modelling work in **Papers I** and **II**. The potential respiration rate measurements for each filter type were also used in the modelling in **Papers I** and **II** to estimate the filter biomass.

3.1.2 Different hydraulic and organic loading regimes

The second experiment consisted of two trials. The filters were first subjected to loading regimes with OLR = 13-16 g BOD_5 m^{-2} day^{-1} and increasing HLR (32, 64 and 128 l m^{-2} day^{-1}) and then to HLR = 32 l m^{-2} day^{-1} and increasing OLR (13-16, 28 and 76 g BOD_5 m^{-2} day^{-1}). This experiment had a total duration of 150 days, with each loading regime running in succession over 3 weeks. It was performed after the filters had been resting for several months following the experiment with fixed hydraulic and organic loads (Figure 3).

Measured influent and effluent concentrations of organic matter for the bark and charcoal filters under the different hydraulic and organic loading rates were later used in the modelling in **Paper II**.

The removal of pollutants in the filters was calculated according to:

$$\text{Removal (\%)} = \frac{C_{in} - C_{out}}{C_{in}} \times 100 \qquad (7)$$

where C_{in} is the influent concentration and C_{out} is the filter effluent concentration of the pollutant. Calculation of removal (%) was also used to evaluate simulated results in **Papers I** and **II**.

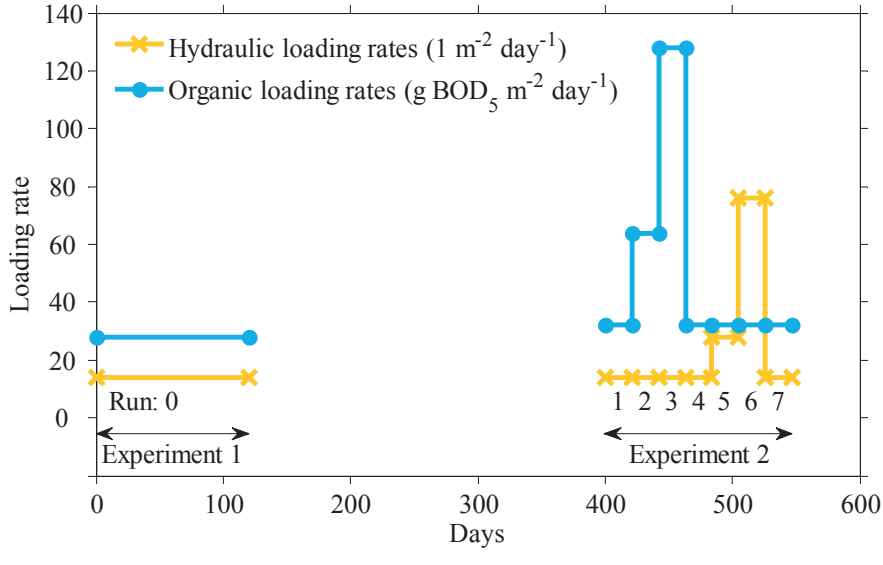

Figure 3. Experimental regime testing different hydraulic and organic loading rates from which input data were obtained for the modelling work presented in this thesis.

3.1.3 Cumulative flow measurements

In order to simulate water transport, there was an additional need for observation of flow through the filters. The cumulative effluent volume was

therefore measured in a separate experiment, which was performed when the filters had been resting for approximately one year after the second experiment.

In this experiment, the filters were loaded with tap water, following the intermittent scheme with three fractions (70, 10 and 20 %) of the total daily load applied at 09.00, 16.00 and 20.00 h, and the filter effluent was collected in a bucket placed on top of a digital scale connected to a computer recording the weight once a minute. This allowed the cumulative effluent volume to be measured.

In the experiment, duplicate columns of each filter type were loaded with 1 l day^{-1} and cumulative effluent was measured over 3-5 days. The columns were then subjected to a double load, 2 l day^{-1}, for 3 more days. However, due to drift in calibration of the dosing device, the loadings were approximately 85% of the expected amount of 1 and 2 l day^{-1} (Karlsson, 2012).
Cumulative effluent measurements were used to estimate parameters for the sand filter flow model in **Paper I** and the bark and charcoal filter flow models in **Paper II**.

3.2 Modelling

3.2.1 Semantics

In this thesis, the HYDRUS wetland module is referred to as 'software'. The term 'modelling' is used for choosing fixed parameter values within the software and a fixed set of parameters make up a 'model'. 'Simulation' is referred to as using the 'model' with different inputs, such as varied HLR or OLR.

3.2.2 Numerical set-up

HYDRUS-2D version 2.01.1240 (Šimůnek *et al.*, 2012) was used for simulating greywater flow through the filters. The transport domain for each filter model was set to a "2D – Simple" geometry, with diameter 20 cm and height 60 cm, to match the experimental set-up with the filter columns (Figure 4).

Following the HYDRUS manual guidelines, the transport domain was discretised into 10 columns and 20 rows, with rows distributed more closely at the top because the top layer of the filter was expected to be critical for the treatment performance. This set-up resulted in a two-dimensional finite element mesh with 231 nodes (60 which were boundary nodes) and 400 triangular finite elements (Figure 4).

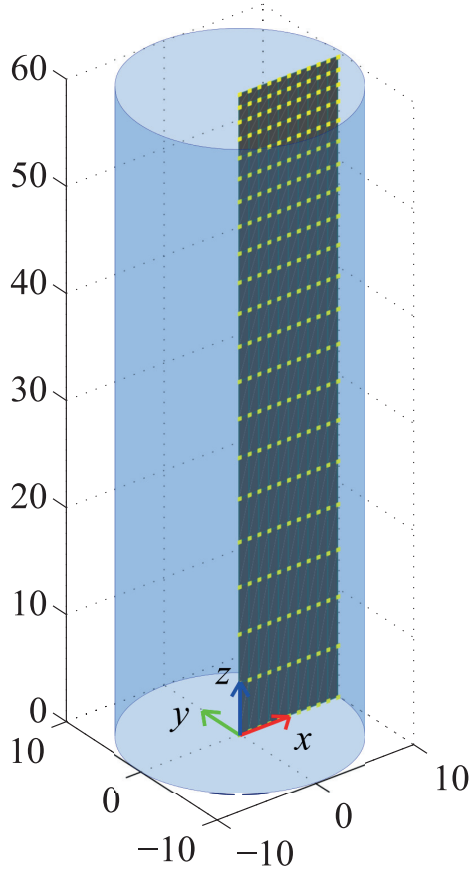

Figure 4. Vertical flow filter model transport domain in "2D – Simple" geometry, 20 x 60 cm (diam. x height), displaying the 231 nodes and 400 triangular finite elements over 10 columns and 20 rows, used in all simulations.

The top layer of the transport domain was assigned an atmospheric boundary condition and the bottom drainage layer a constant pressure head boundary condition (-2 cm). The time resolution was set to minutes, with a minimum and maximum time step of 0.00001 and 1 minute, respectively, which are the HYDRUS default values. However, in the settings, it was specified that the output should be printed out as only one value per minute, to give a data set equal to the flow measurements, which were recorded once a minute. For details of numerical set-up not mentioned here, the study followed the HYDRUS manual guidelines (Šimůnek *et al*., 2001).

The numerical set-up as described here was used in modelling the sand filter in **Paper I** and the bark and charcoal filters in **Paper II**.

3.2.3 Flow parameter estimation

To model the hydraulic properties of the sand filter in **Paper I**, flow parameters were estimated by utilising the built-in inverse simulation function of HYDRUS-2D, which produces the optimal estimates of the selected fitting parameters through a Marquardt-Levenberg type parameter estimation technique (Šimůnek *et al.* 2012). This was also done for the bark and charcoal filters in **Paper II**.

The cumulative effluent data for each filter type were calculated to a mean one-day time series from the duplicate filters and five-day measurements. This one-day time series was set as the objective function (*i.e*. cumulative effluent data as a function of time constituted the objective function). The objective function corresponded to 1440 data points (one measurement per minute for 24 hours) for the inverse simulation of sand and bark filter flow parameter estimation. For estimating parameters for the charcoal filter the inverse simulation did not converge. Therefore, the objective function was cut to include only the first 400 minutes during which the first loading (70% of daily amount) took place.

The inverse simulation function requires initial values to be specified for the parameters to be estimated. Different initial values for each estimated parameter were tested and the best result selected using the "Inverse Solution Results" tab in HYDRUS, which gives the correlation matrix and various goodness-of-fit measures. This same procedure was applied for the sand filter model in **Paper I** and for the bark and charcoal models in **Paper II**.

In **Paper I**, varying the degree of flow model calibration was tested through increasing the number of fitting parameters. This was done by first using zero fitting parameters (*i.e.* the default values available in HYDRUS), then fitting the inverse air entry value and pore connectivity parameters for a second model. A suspected effect of water flowing faster along the column wall was also included in a third model to investigate whether this improved the fit. This was done with specifying a second material in the transport domain to make up a 'wall layer' (Figure 5). For the 'wall layer', all hydraulic parameters (seven in total) were estimated in the model.

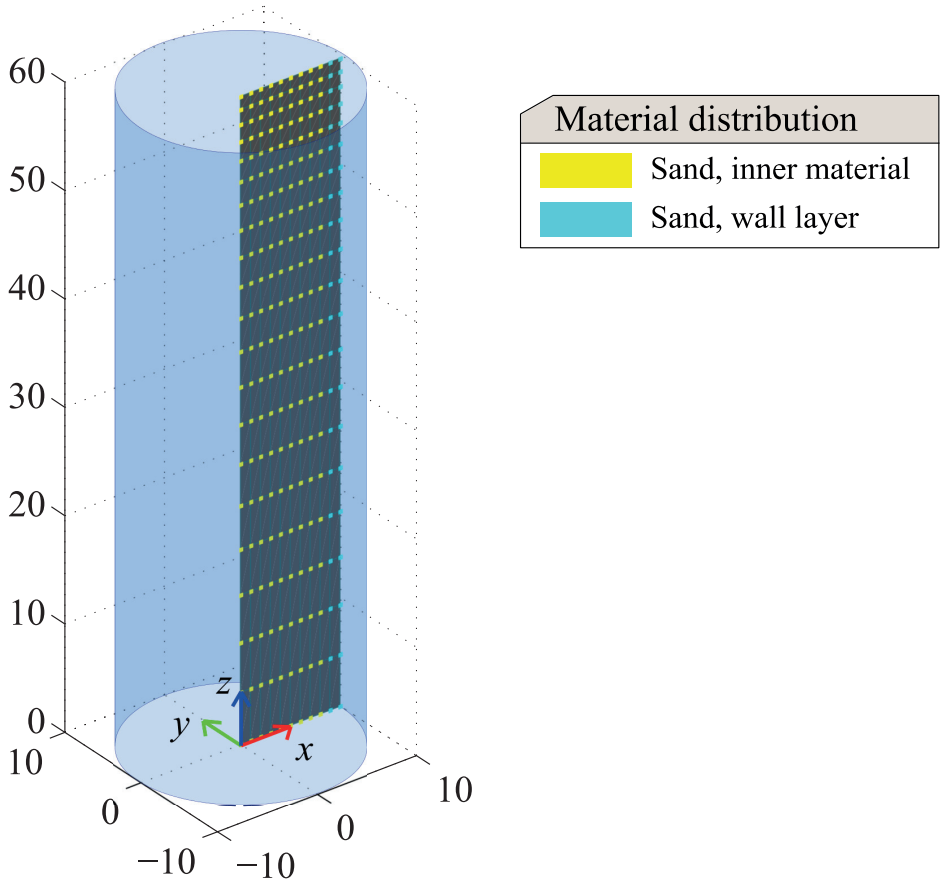

Figure 5. Sand filter model 3 transport domain in "2D – Simple" geometry, 20 x 60 cm (diam. x height), displaying the 231 nodes and 400 triangular finite elements (over 10 columns and 20 rows) and the material distribution (inner filter material and outer wall layer).

The estimated flow model parameters in **Papers I** and **II** were validated by using them to simulate a hydraulic load that was approximately twice the volume of the original load. The simulated results were then compared with observations (using one-day mean time series) and goodness-of-fit measures were calculated.

3.2.4 Biological degradation of organic matter

For the studies in **Papers I** and **II**, the HYDRUS wetland module with the CW2D setting chosen was used to simulate the degradation of organic matter inside the filters once the flow model had been calibrated.

To assess the microbial activity, substrate-induced potential respiration rate observations were analysed during the 112-day initial experiment (Run 0) as

described in Dalahmeh *et al.* (2014a). For the modelling, it was assumed that the filters were operating under approximate steady-state conditions for the 112-day initial experiment (Run 0). Therefore, the potential respiration rate (measured on four occasions) was calculated as a mean value for each depth (0-2, 20, 40 and 60 cm).

Since the HYDRUS wetland module describes microbial activity with units µg COD g material^{-1}, the measured mean potential respiration rate (mg O_2 l^{-1} day^{-1}) had to be converted before being used to calibrate the growth of heterotrophic biomass (*XH*, µg COD g material^{-1}) in the model. The measured mean values of respiration rates were converted to µg biomass COD g material^{-1} using empirical equations 8 and 9, from Anderson and Domsch (1977) and Langergraber *et al*. (2007), respectively:

$$\mu g \text{ biomass C g material}^{-1} = (\mu l\ CO_2 \text{ g material}^{-1} h^{-1}) \times 40.04 + 0.37 \quad (8)$$

$$\mu g \text{ biomass COD g material}^{-1} = 2.667\ (\mu g\ O_2) \times (\mu g \text{ biomass C g material}^{-1}) \quad (9)$$

The initial level of heterotrophic biomass in each filter model was set as the estimated mean value of filter biomass at each depth (0-2, 20, 40 and 60 cm). A linear relationship was used to interpolate the values between the measured depths. Model parameters limiting microbial growth, the heterotrophic lysis rate constant (b_H, day^{-1}) and maximum aerobic growth rate (μ_H, day^{-1}), were adjusted to set values that ensured simulated biomass (*XH*) matched observations and did not grow excessively during simulations (1-5 simulated days). With the HYDRUS wetland module, it is not possible to calibrate so that *XH* stays entirely constant or to impose a maximum threshold.

Both **Paper I** and **Paper II** used the method described here to calibrate the growth of heterotrophic biomass to match the observed microbial activity in the filter materials.

3.2.5 Specifying the influent greywater composition

In CW2D, total COD is divided into three fractions: readily biodegradable soluble COD (*CR*), slowly biodegradable soluble COD (*CS*) and inert soluble COD (*CI*). When specifying the COD of the greywater into these three COD fractions as input for the models, different approaches were used in **Paper I** and **Paper II**.

In **Paper I**, considering the ingredients of the artificial greywater as described by Dalahmeh *et al.* (2012), *CI* was estimated to constitute 10% of the measured COD concentration. Furthermore, it was assumed that *CR* corresponded to the measured BOD_5 concentration, since *CR* is the fraction of organic matter that is readily accessible to the microbes. *CS* is a more slowly

degradable fraction of the substrate and was chosen to correspond to the remaining amount of COD.

In **Paper II**, the *CI* was estimated for each loading regime as 0.5 times the outgoing COD concentration of the charcoal filter. This was done in agreement with other studies, where *CI* was chosen as a factor 0.5-0.9 times the COD effluent concentration (Dittmer *et al.*, 2005; Henrichs *et al.*, 2007; Langergraber *et al.*, 2007; Toscano *et al.*, 2009). The outgoing COD concentration of the bark filter was not used because the bark filter released COD from the bark material itself, which would give a bias. The bark influent fractionation was therefore assumed to equal the estimated influent fractionation for the charcoal filter.

The *CR* and *CS* were then estimated according to the formula *CR* = 2 x *CS*, also according to the studies cited (Dittmer *et al.*, 2005; Henrichs *et al.*, 2007; Langergraber *et al.*, 2007; Toscano *et al.*, 2009).

In this thesis, the initial experiment with HLR = 32 l m^{-2} day^{-1} and OLR = 14 g BOD_5 m^{-2} day^{-1} is denoted Run 0 (Table 1). The initial experiment was simulated with the sand filter model in **Paper I** and with the bark and charcoal filter models in **Paper II**.

Out of the seven loading regimes in the second experiment, only three regimes were simulated in **Paper II** with the bark and charcoal filter models. The simulated regimes are denoted here (as in **Paper II**) Run 1, Run 2 and Run 5, following the order in which the regimes were conducted in the experiment (Figure 3). Run 1 had a HLR of 32 l m^{-2} day^{-1} and an OLR of 13 - 16 g BOD_5 m^{-2} day^{-1}, Run 2 had a HLR = 64 l m^{-2} day^{-1} and an OLR of 14 g BOD_5 m^{-2} day^{-1} and Run 5 had a HLR of 32 l m^{-2} day^{-1} and an OLR of 28 g BOD_5 m^{-2} day^{-1} (Table 1). The most extreme loading regimes (Runs 3 and 6) were not simulated, and the remaining loading regimes (Runs 4 and 7) were duplicate regimes of Run 1.

Although Run 0 and Run 1 had similar OLR in terms of BOD_5, the mean influent COD concentration differed between the two (885 ± 127, n = 2 and 1450 ± 470, n = 4 respectively, mean value ± standard deviation, Table 1).

Table 1. *Influent greywater concentrations (mean ± standard deviation) in the different loading regimes: Run 0, Run 1, Run 2 and Run 5 of the measured BOD_5 and COD and calculated CR, CS and CI*

Parameter (abbrev., unit)	Run 0	No. of samples for Run 0	Run 1	Run 2	Run 5	No. of samples for Runs 1, 2 and 5
Hydraulic loading rate (HLR, l m^{-2} day^{-1})	32	-	32	64	32	-
Organic loading rate (OLR, g BOD_5 m^{-2} day^{-1})	14	-	13-16	14	28	-
Readily biodegradable organic matter (*CR*, mg l^{-1})	574	-	913	494	1879	-
Slowly biodegradable matter (*CS*, mg l^{-1})	287	-	457	247	940	-
Inert organic matter (*CI*, mg l^{-1})	24	-	80	39	241	-
Biochemical oxygen demand (BOD_5, mg l^{-1})	425 ± 152	12	490 ± 49	198 ± 13	875 ± 452	2
Chemical oxygen demand (COD, mg l^{-1})	885 ± 127	2	1450 ± 470	780 ± 110	3060 ± 830	4

3.2.6 Time-span and initial conditions

Because of the excessive increase in heterotrophic biomass (*XH*) over time in the models, the simulated time span was not set to equal the experimental time span (112 days for the initial experiment and 3 weeks for each loading regime in the second experiment). In **Paper I**, the sand filter model was set to simulate 24 hours, representing an arbitrary day towards the end of the initial 112-day experiment. Initial conditions for all model components except *XH* were imported from the last time layer of a 20-day simulation where pseudo steady state had been reached.

In **Paper II**, the simulation time span was set to 5 days for each loading regime, in contrast to the experimental run period of 112 days for Run 0 and 3 weeks each for Runs 1, 2 and 5.

For initial conditions, Run 0 was re-simulated once with the conditions of the last simulated time layer as initial conditions. Initial conditions for Run 1 were set to match the conditions of the last simulated time layer of Run 0. For both Run 2 and Run 5, initial conditions were set to match the conditions of the last simulated time layer of Run 1, since in the experimental scheme the loading regime preceding Run 5 was identical that preceding Run 1.

3.3 Goodness-of-fit measures

Assessment of the quality of the model fit achieved is required in all modelling work (Moriasi *et al.*, 2012; Ahnert *et al.*, 2007). Both **Paper I** and **Paper II** followed the recommendations for goodness-of-fit measures for numerical modelling in urban water management by Ahnert *et al.* (2007). The recommendations are to make a visual evaluation, such as a time series, and to use Coefficient of Efficiency (*E*) as a goodness-of-fit measure.

E ranges from -∞ to 1, with $E = 1$ indicating a perfect fit. *E* is calculated according to:

$$\mathrm{E_j} = 1 - \frac{\sum_{i=1}^{N} |O_i - P_i|^j}{\sum_{i=1}^{N} |O_i - \bar{O}|^j} \quad (10)$$

where *O* is the observed value, *P* is the model prediction and N is the number of observations. When $j = 2$, this equation becomes the original equation given for *E* by Nash and Sutcliffe (1970). Using $j = 1$ gives the modified *E* usually denoted in the literature as E_1, which was first presented by Legates and McCabe (1999). The modified *E* is recommended over the original with $j = 2$, because the original *E* reaches high values even with mediocre modelling results. Thus, in this thesis and in **Papers I** and **II**, *E* with $j = 1$ was used, and referred to as *E*.

The Index of Agreement (*d*) was also used as a goodness-of-fit measure in both **Paper I** and **Paper II** and was calculated according to:

$$\mathrm{d_j} = 1 - \frac{\sum_{i=1}^{N} |P_i - O_i|^j}{\sum_{i=1}^{N} (|P_i - \bar{O}| + |O_i - \bar{O}|)^j} \quad (11)$$

where *O* is the observation, *P* is the model prediction and *N* is the number of observations. When $j = 2$, this equation becomes the original equation published by Willmott (1981). However, as this formula was increasingly used for evaluating model performance, a suspicion arose that squaring the errors prior to summing them was causing a numerical problem. Willmott *et al.* (1985) therefore suggested a new version, d_1, which is calculated with $j = 1$. This modified *d* has since been preferred over the original *d* with $j = 2$, because it provides greater separation when comparing models that perform relatively well and is much less sensitive to the shape of the error frequency distribution (meaning less sensitivity to errors concentrated in outliers). Thus, in both this thesis and in **Papers I** and **II**, *d* with $j = 1$ was used, and referred to as *d*.

Besides *E* and *d*, the Root Mean Square Error (*RMSE*) between observed and modelled data was calculated in both **Paper I** and **Paper II**. To facilitate comparison between the *RMSE* of simulations of different hydraulic loading

rates, the Normalised Root Mean Square Error (*NRMSE*), *i.e.* the *RMSE* divided by the range of observed values, was also determined.

3.4 Sensitivity analysis of filter models

A sensitivity analysis was performed on each filter model in order to determine the relationships between model parameters and the simulated COD and to identify the parameters with the largest impact on simulated organic matter degradation. Evaluating the effect on model outputs exerted by individually varying one of the model parameters at a time across a range of values, while holding all other parameters at their nominal or base-scenario values, is a method called Nominal Range Sensitivity Analysis (NRSA) (Cullen & Frey, 1999). The difference in the model output due to the change in the input variable compared with the base scenario output is referred to as the sensitivity of the model to the varied parameter (Morgan & Henrion, 1990).

To check the sensitivity of the bark, charcoal and sand filter models, NRSA was performed. The base scenario was set as the chosen parameters for each filter model. Each parameter was varied as 0.5, 0.8, 0.9, 1.1, 1.2 and 1.5 times the base scenario value.

For the bark and charcoal filter models, 51 parameters were varied in 306 simulations. For the sand filter model, which had a second material specified for the simulation of wall flow effects, a total of 57 parameters were varied in 342 simulations. To carry out the simulations for the NRSA automatically, a script was created that manipulated the input variables in the HYDRUS wetland module input files. The sensitivity was calculated as positive (or negative) percentage change compared with the base scenario effluent COD.

When the mean of the absolute value percentage changes in effluent COD concentrations for a particular parameter (varied as 0.5, 0.8, 0.9, 1.1, 1.2 and 1.5 times its base scenario value) was larger than 3%, the model was considered sensitive to that particular parameter.

4 Results

4.1 Simulated filter column flow

The parameter values used for the sand filter material (**Paper I**) are presented together with the parameter values used for the bark and the charcoal filter materials (**Paper II**) in Table 2.

Table 2. *Default (*), measured (**) and estimated (unmarked) water flow parameters used for the models of bark, charcoal and sand filters when simulating with the HYDRUS wetland module*

Parameter (abbrev., unit)	Bark filter model	Charcoal filter model	Sand filter model, inner material	Sand filter model, wall material
Residual soil water content (θ_r,-)	0.045*	0.045*	0.045*	0.001
Porosity (θ_s, -)	0.41 (0.73**)	0.14 (0.85**)	0.34**	0.28
Inverse air entry value, α (cm^{-1})	0.0694	0.3746	0.1007	0.0609
Pore connectivity parameter, n (-)	5.818	1.596	3.333	4.829
Saturated hydraulic conductivity, K_s ($cm\ h^{-1}$)	330*	500*	360*	3720

The estimation of selected hydraulic parameters resulted in a close fit between simulated and measured cumulative effluent, with the best fit seen for the sand and charcoal models (Figure 6a). The close fit was further demonstrated by viewing the residuals, which were largest for bark but close to zero for the sand and charcoal models (Figure 6b).

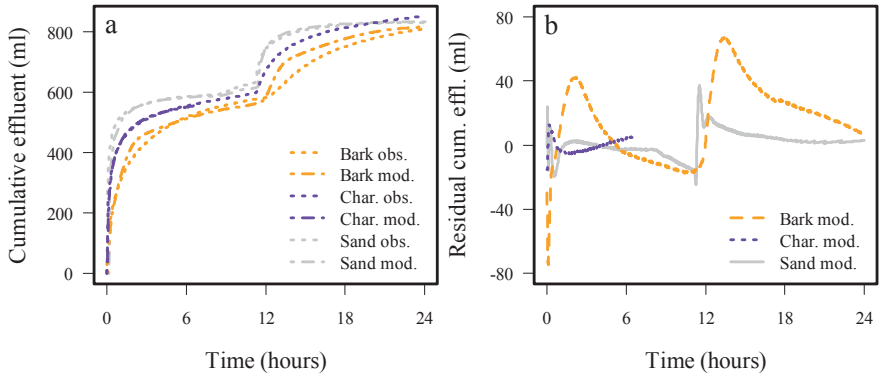

Figure 6. (a) Observed and simulated cumulative effluent volume as a function of time for the bark, charcoal and sand filter models and *(b)* calculated residual of simulated cumulative effluent volume compared with observed values for the bark, charcoal and sand filter models.

4.1.1 Sand filter wall flow effect

In **Paper I**, the first sand filter model with standard hydraulic parameters for sand resulted in moderate agreement between simulated and measured cumulative effluent values (Sand mod. 1, Figure 7a). Estimating the inverse air entry value α and the pore connectivity parameter n in a second sand filter model improved the fit (Sand mod. 2, Figure 7a). The improved fit was also demonstrated by decreased residuals (Figure 7b). Introducing wall flow effects in a third sand filter model by setting a 1 cm thick wall layer with all parameters estimated (Figure 5) further improved the fit between simulated and observed values (Sand mod. 3, Figure 7a). The estimation was done using the HYDRUS inbuilt inverse simulation tool, as explained in section 3.2.3. The resulting parameter values of the three different sand models are given in Table 3.

Models with estimated parameters were better at simulating cumulative effluent in terms of all fitness measures than using a model with standard parameters (Table 4). Sand model 3 with inclusion of wall flow effects gave the best fit (Table 4).

Table 3. *CW2D water flow parameters in sand filter test models, default (*), measured (**) and estimated (unmarked) values* ***(Paper I)***

Parameter (abbrev., unit)	Sand model 1, standard parameter set	Sand model 2, est. α and n	Sand model 3, est. α and n, inner material	Sand model 3, est. α, n, θ_r, θ_s, and K_s, wall material
Residual soil water content (θ_r,-)	0.045*	0.045*	0.045*	0.001
Porosity (θ_s, -)	0.34**	0.34**	0.34**	0.28
Inverse air entry value, α (cm^{-1})	0.1450	0.0516	0.1007	0.0609
Pore connectivity parameter, n (-)	2.680	3.196	3.333	4.829
Saturated hydraulic conductivity, K_s ($cm\ h^{-1}$)	360*	360*	360*	3720

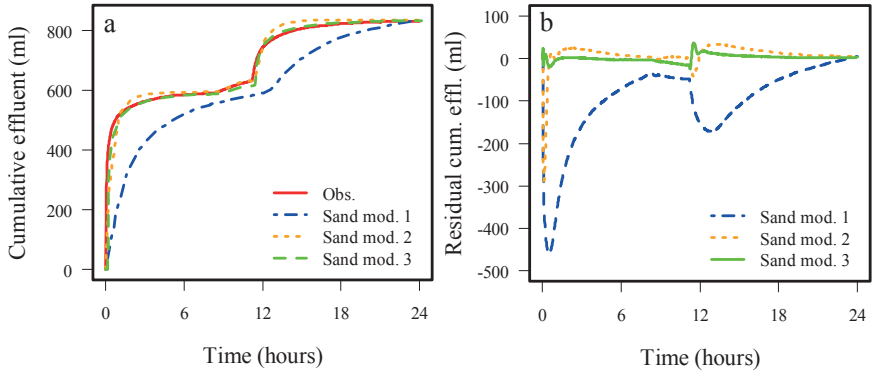

Figure 7. (a) Observed (Obs.) and simulated cumulative effluent volume as a function of time for Sand model 1 (standard parameters used), Sand model 2 (parameters estimated from inverse simulation) and Sand model 3 (parameters estimated from inverse simulation including wall flow effects) and *(b)* calculated residual of simulated cumulative effluent volume compared with observed values for Sand models 1-3 (**Paper I**).

4.1.2 Validation of flow models

The sand filter model (**Paper I**) and the bark and charcoal filter models (**Paper II**) were all able to simulate a doubled hydraulic load, with a close fit to the corresponding measured cumulative effluent volume (Figures 8a-c).

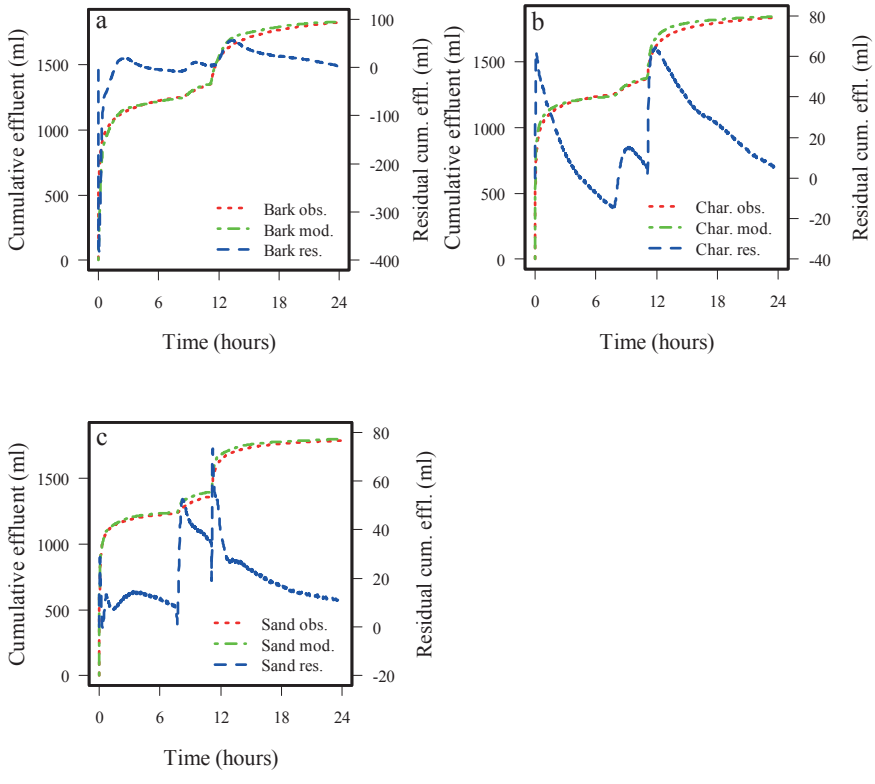

Figure 8. Observed and simulated cumulative effluent volume and calculated residual cumulative effluent volume with a doubled hydraulic load for *(a)* the bark filter model, *(b)* the charcoal filter model and *(c)* sand filter model 3.

4.1.3 Flow model goodness-of-fit

The goodness-of-fit measures for the sand filter models were calculated in **Paper I** and for the bark and charcoal filter models in **Paper II**. In general, the fit of simulated results compared with observations was good for all filter models (Table 4).

When the flow models were used to simulate a doubled hydraulic load and the results were compared with measured data, the goodness-of-fit measures for all filter models demonstrated E equal to 0.92 and d equal to 0.96.

The normalised *RMSE* ranged from 0.7-3.7% in all simulations where the filter models had estimated parameters. The only model with no estimated parameters, Sand model 1, which used HYDRUS wetland module standard values, had a normalised *RMSE* of 16.4%.

Table 4. *Goodness-of-fit measures for cumulative effluent simulations for the sand filters (**Paper I**), bark and charcoal filters (**Paper II**) for both calibration data and validation data with doubled hydraulic load*

Goodness-of-fit measure (unit)	Bark model	Bark model, validation	Charcoal model	Charcoal model, validation	Sand model 1, standard parameters used	Sand model 2, parameters estimated from inverse simulation	Sand model 3, parameters estimated from inverse simulation incl. wall flow effects	Sand model 3, parameters estimated from inverse simulation incl. wall flow effects, validation
Amount loaded (ml day^{-1})	810	1827	852*	1840	831	831	831	1786
Min and max error (ml)	- 75, + 67	- 387, + 56	- 14, + 13	- 15, + 64	- 462, + 5	- 288, + 34	- 24, + 37	- 1, + 73
Root Mean Squared Error, *RMSE*	28	42	4	29	136	31	8	24
Normalised *RMSE* (%)	3.5	2.3	0.7	1.6	16.4	3.7	1.0	1.3
Coefficient of Efficiency, *E*	0.82	0.919	0.993	0.917	0.18	0.86	0.95	0.922
Index of Agreement, *d*	0.91	0.961	0.993	0.959	0.66	0.93	0.99	0.961

*Total load for the evaluation period was 528 ml

4.2 Simulated biomass

The heterotrophic biomass parameters b_H and μ_H (heterotrophic lysis rate constant and maximum aerobic growth rate, respectively) were calibrated for all three filter models (bark, charcoal and sand; Table 5). For the sand filter model (**Paper I**) the simulated biomass (*XH*) in Run 0 corresponded well to the observed value. A difference in simulated biomass concentration between the inner sand filter material and the outer wall layer was noted. For the charcoal filter model, the simulated biomass in Run 0 remained at fairly constant levels close to the observed values over the simulated five-day time span. The bark filter model demonstrated overestimation of biomass when simulating Run 0, primarily in the top 0-20 cm of the filter (Figures 9a & b).

Table 5. *Calibrated model heterotrophic biomass parameters for the sand filter model in* ***Paper I*** *and the bark and charcoal filter models in* ***Paper II***

Parameter (abbrev., unit)	Bark filter model	Charcoal filter model	Sand filter model	Default values
Heterotrophic lysis rate constant (b_H, min^{-1})	0.0005	0.0005	0.0003	0.00027
Maximum aerobic growth rate (μ_H, min^{-1})	0.005	0.003	0.003	0.0042

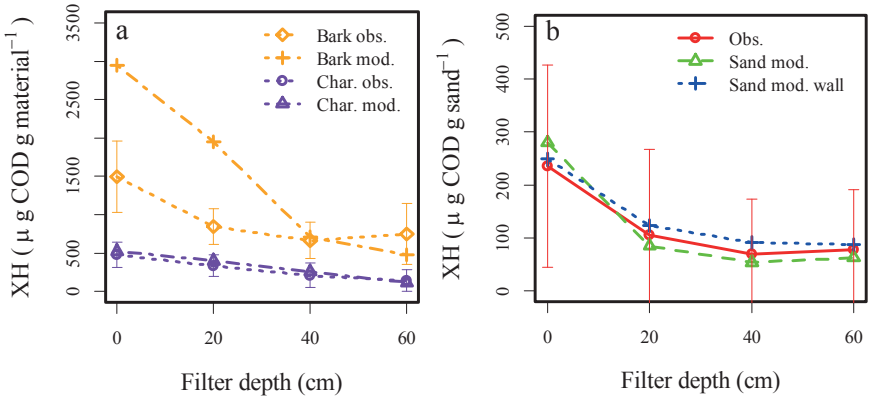

Figure 9. Observed (error bars display standard deviations, n = 10) and simulated concentration of heterotrophic microorganisms (*XH*) for Run 0 at filter depths 0, 20, 40 and 60 cm in *(a)* the bark and charcoal filter models, mean values taken during the five-day simulation time span (**Paper II**) and *(b)* the sand filter model, simulated mean values taken from centre of filter and from the wall layer (Sand mod. wall) during the one-day simulation time span (**Paper I**).

4.2.1 Simulated biomass under increased HLR and OLR

The results of the model simulations showed an increase in biomass (*XH*) in the two top layers of the bark and charcoal filters with increasing OLR (Figures 10a & b; **Paper II**). For the bark filter, *XH* also tended to increase when HLR increased, as can be seen on comparing Run 1 and Run 2 (Figure 10a). However, this was not the case for the charcoal filter, where the *XH* remained fairly constant for both Run 1 and Run 2 (Figures 10a & b).

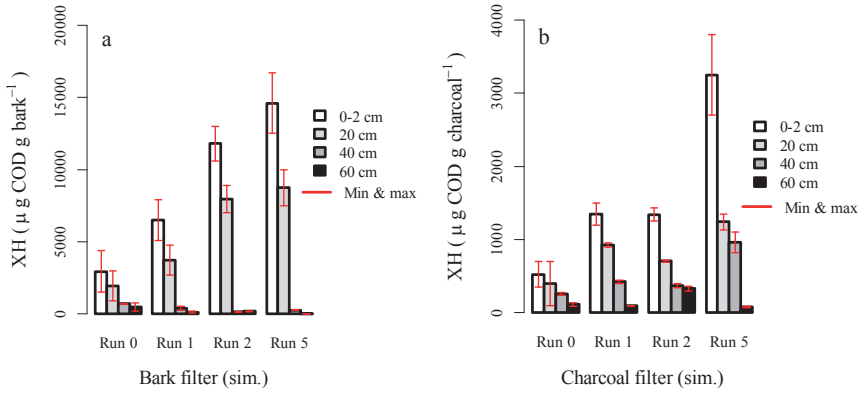

Figure 10. Mean simulated filter concentration of heterotrophic microorganisms (*XH*, error bars indicate the range) at filter depths 0-2, 20, 40 and 60 cm for different hydraulic and organic loading rates (Run 0: HLR = 32 l m^{-2} day^{-1}, OLR = 14 g BOD_5 m^{-2} day^{-1}; Run 1: HLR = 32 l m^{-2} day^{-1}, OLR = 13-16 g BOD_5 m^{-2} day^{-1}; Run 2: HLR = 64 l m^{-2} day^{-1}, OLR = 14 g BOD_5 m^{-2} day^{-1}; Run 5: HLR = 32 l m^{-2} day^{-1}, OLR = 28 g BOD_5 m^{-2} day^{-1}), simulated for 5 days with *(a)* the bark filter model and *(b)* the charcoal filter model (**Paper II**).

4.3 Simulated organic matter degradation

Both **Paper I** and **Paper II** included simulation of organic matter degradation in the filters. In **Paper I**, the sand filter demonstrated a simulated effluent COD concentration of 338 mg l^{-1} which was higher than the measured 245 ± 106 mg l^{-1} but well within the standard deviation of the measurement. In **Paper II**, the simulated bark filter effluent concentration of COD (92 mg l^{-1}) was less than the measured value (200 ± 7 mg l^{-1}). The simulated charcoal filter effluent concentration of COD (57 mg l^{-1}) was consistent with the measured value (48 ± 11 mg l^{-1}) (Figure 11).

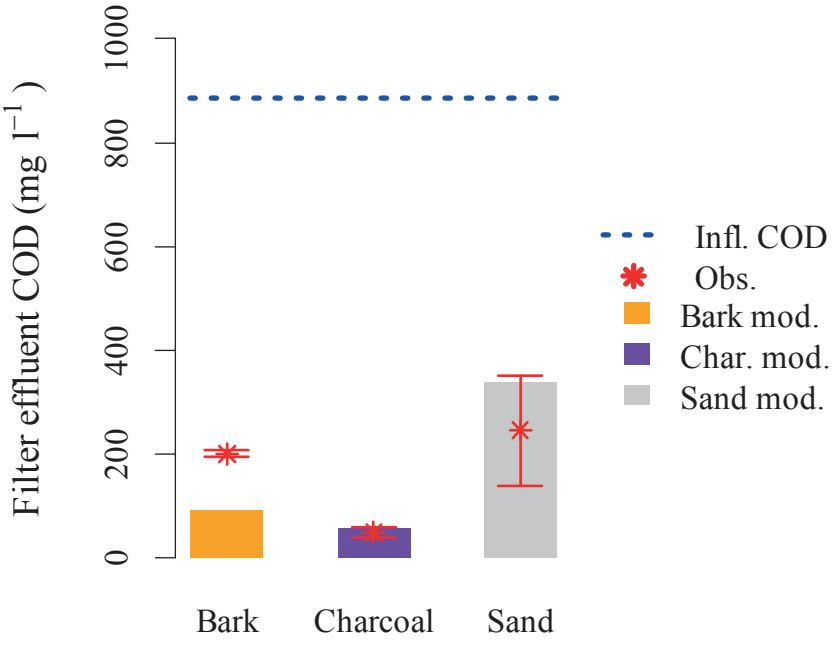

Figure 11. Simulated mean effluent COD concentration and observed values (*, bars represent standard deviations, n = 4) in effluent from the bark, charcoal and sand filters compared with average influent COD concentration (---, mg l^{-1}).

In **Paper I**, different sand filter models with varying degrees of calibration of flow model parameters were tested. The results were then compared against each other, with the best fitting sand filter model also used for a simulation with increased biomass levels.

The simulated results indicated that the sand filter model without wall flow effects underestimated the effluent COD compared with the measured effluent concentration (Sand model 2, Table 6). The simulated effluent COD consisted mainly of the *CI* fraction. The simulated *CR* fraction, expected to correspond to measured BOD_5, was greatly underestimated (Sand model 2, Table 6). Simulation with the sand filter model including wall flow effects, on the other hand, slightly overestimated the total organic matter concentration in the effluent compared with measured values. However, the simulated effluent *CR* compared well with measured BOD_5 (S.Mod. 3, Table 6).

When the sand filter model including wall flow effects was modified as having more biomass, less COD was present in the effluent. This reduction in effluent concentration of organic matter was mainly seen for the *CR* fraction (Table 6).

Table 6. *Observed (Obs.) mean sand filter influent (Infl.) and effluent concentrations of BOD_5 and COD (Dalahmeh et al., 2012) and the simulated organic matter content of three sand filter models (**Paper I**).*

Parameter (abbrev.)	Infl. concentrations (mg l^{-1})		Effluent concentrations (mg l^{-1})			
	Obs.	Sim.	Obs.	Sim.		
				Sand mod. 2	Sand mod. 3	Sand mod. 3, incr. biomass
Readily biodegradable organic matter (*CR*)	-	425	-	2	139	94
Slowly biodegradable organic matter (*CS*)	-	374	-	6	98	94
Inert organic matter (*CI*)	-	86	-	125	101	112
Biochemical oxygen demand (BOD_5)*	425 ± 56	-	108 ± 57	2	139	94
Chemical oxygen demand (COD)**	885 ± 130	885	245 ± 106	133	338	300

*Mean ± standard deviation, n = 24.
** Mean ± standard deviation, n = 4.

4.3.1 Simulated organic matter under increased HLR and OLR

In **Paper II**, the bark and charcoal filter models simulated the effluent concentrations of pollutants under the varying loading regimes. The bark filter model overestimated the COD removal in all loading regimes by 13-20 percentage points compared with measured values (Figure 12).

The charcoal filter model, on the other hand, simulated the COD removal accurately relative to measured values for Run 0 and Run 1 (94 and 91 % compared with observed 95 ± 2 and 89 ± 11 %, respectively). For Run 2 and Run 5, the simulated COD removal of the charcoal filter model was 70 and 72 %, respectively, meaning underestimation of removal by 20 and 12 percentage points compared with the observed 90 ± 7 and 84 ± 4, respectively (Figure 12).

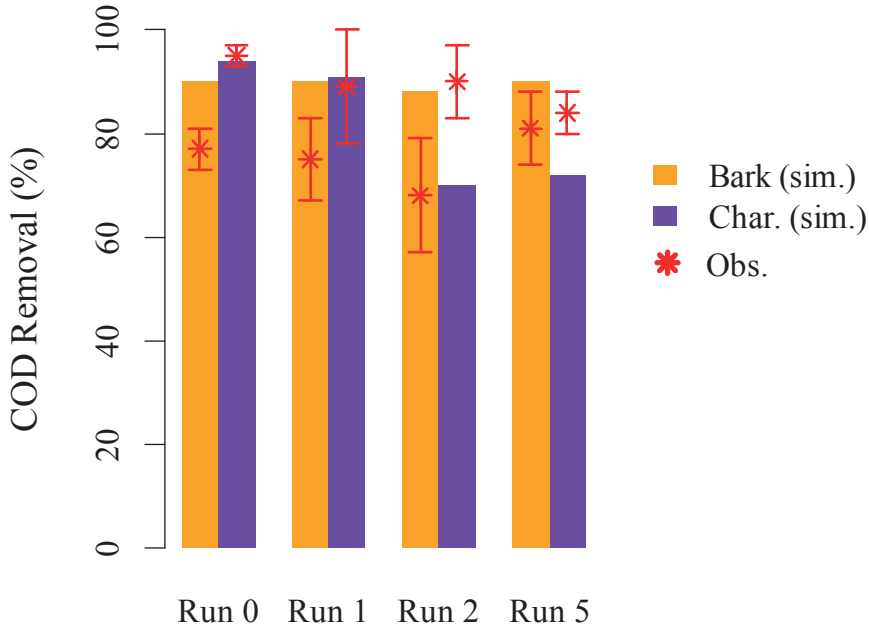

Figure 12. Simulated and observed (*, bars represent standard deviations, n = 4) bark and charcoal filter COD removal (%) in four loading regimes: Run 0: HLR = 32 l m^{-2} day^{-1}, OLR = 14 g BOD_5 m^{-2} day^{-1}; Run 1: HLR = 32 l m^{-2} day^{-1}, OLR = 13-16 g BOD_5 m^{-2} day^{-1}; Run 2: HLR = 64 l m^{-2} day^{-1}, OLR = 14 g BOD_5 m^{-2} day^{-1}; Run 5: HLR = 32 l m^{-2} day^{-1}, OLR = 28 g BOD_5 m^{-2} day^{-1} (**Paper II**).

4.4 Sensitivity analysis

The sensitive parameters for COD effluent concentration simulation identified for each filter model are summarised in Table 7 and detailed results for each filter model are described in the following sections. The complete results of the NRSA can be found in Appendix B.

Table 7. *Sensitive model parameters for simulation of COD effluent concentration*

	Parameter abbreviation and description (unit)	Noted filter model sensitivity*			
		Bark	Charcoal	Sand	
				Inner material	Wall layer
α	Inverse air entry value (cm^{-1})	x	x	x	x
n	Pore connectivity (-)	x	x	x	x
θ_s	Porosity (-)	x	x	x	x
θ_r	Residual soil water content (-)	x	x	x	
K_s	Saturated hydraulic conductivity (cm h^{-1})				x
b_H	Heterotrophic bacteria rate constant for lysis (h^{-1})	x	x	x	
$f_{BM,CI}$	Fraction of CI generated in biomass lysis (-)	x	x	x	
Y_{Het}	Yield coefficient for XH (-)	x	x	x	
K_h	Hydrolysis rate constant (h^{-1})	x	x		
K_X	Saturation/inhibition coefficient for hydrolysis (-)		x		
μ_H	Maximum aerobic growth (h^{-1})			x	
$i_{N,\,BM}$	N content of biomass (-)			x	

* When the mean of the absolute value percentage changes in simulated effluent COD concentrations was larger than 3 % for a particular parameter (parameter varied as 0.5, 0.8, 0.9, 1.1, 1.2 and 1.5 times its base scenario value).

4.4.1 Bark filter model

The NRSA showed that the bark filter model demonstrated sensitivity to mainly material parameters, in particular the inverse air entry value (α) but also the heterotrophic bacteria rate constant for lysis (b_H) and the fraction of CI generated in biomass lysis ($f_{BM,CI}$, Figure 13).

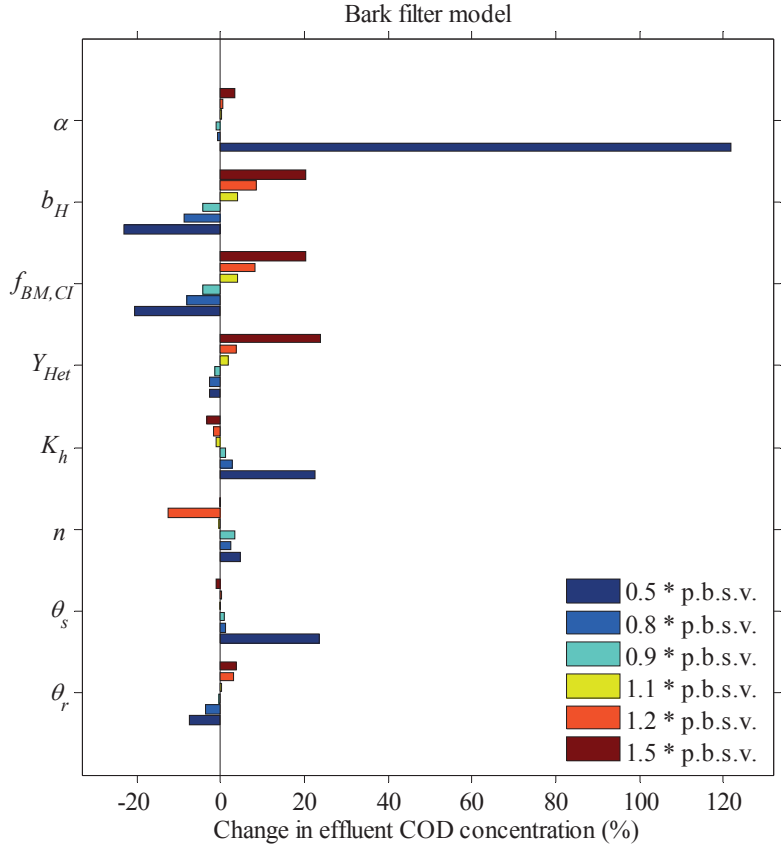

Figure 13. Simulated percentage change in effluent COD concentration for simulations with selected bark model parameters varied one at a time as 0.5, 0.8, 0.9, 1.1, 1.2 and 1.5 times the parameter base scenario value (p.b.s.v.). Selection based on when the mean of the absolute percentage change in simulated effluent COD concentrations was larger than 3 % for a particular parameter (varied as 0.5, 0.8, 0.9, 1.1, 1.2 and 1.5 times its p.b.s.v.).

4.4.2 Charcoal filter model

The charcoal filter model demonstrated inordinate sensitivity to the yield coefficient for *XH* (Y_{Het}). The material parameter determining porosity also demonstrated excessive sensitivity when decreased by 50% (θ_s; Figure 14). The charcoal filter model was the only model demonstrating sensitivity to the saturation/inhibition coefficient for hydrolysis (K_X; Table 7).

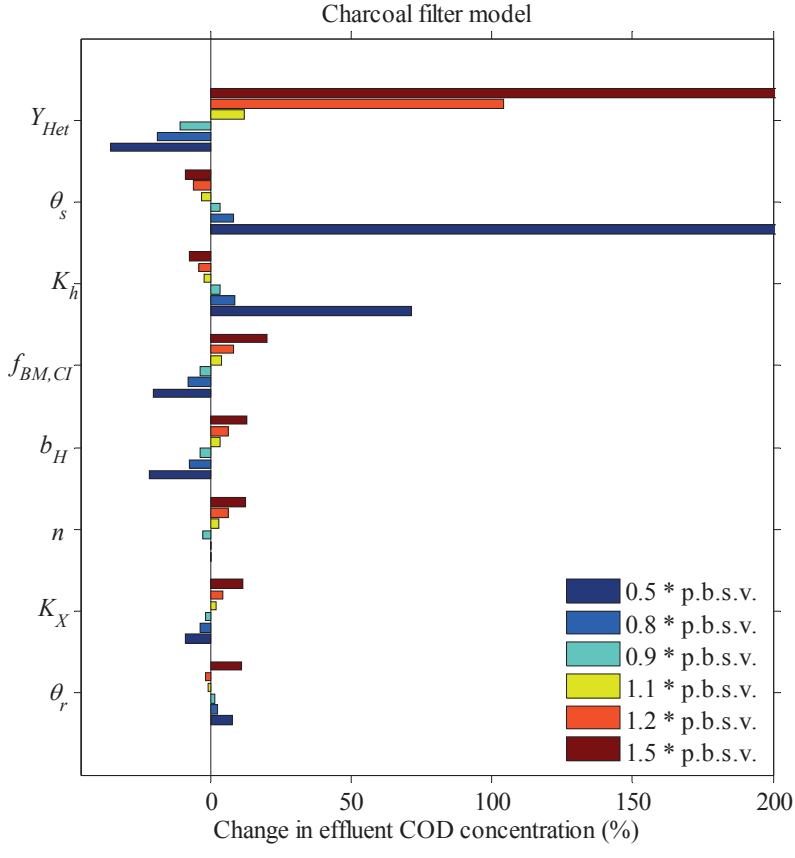

Figure 14. Simulated percentage change in effluent COD concentration for simulations with selected charcoal model parameters varied one at a time as 0.5, 0.8, 0.9, 1.1, 1.2 and 1.5 times the parameter base scenario value (p.b.s.v.). Selection based on when the mean of the absolute percentage change in simulated effluent COD concentrations was larger than 3 % for a particular parameter (varied as 0.5, 0.8, 0.9, 1.1, 1.2 and 1.5 times its p.b.s.v.).

4.4.3 Sand filter model

The sand filter model demonstrated sensitivity mainly to parameters concerning hydraulic properties of the filter material (Figure 15). The sand filter model was the only model demonstrating sensitivity to the saturated hydraulic conductivity (K_s), the maximum aerobic growth (μ_H) and the biomass N content ($i_{N,\,BM}$; Table 7).

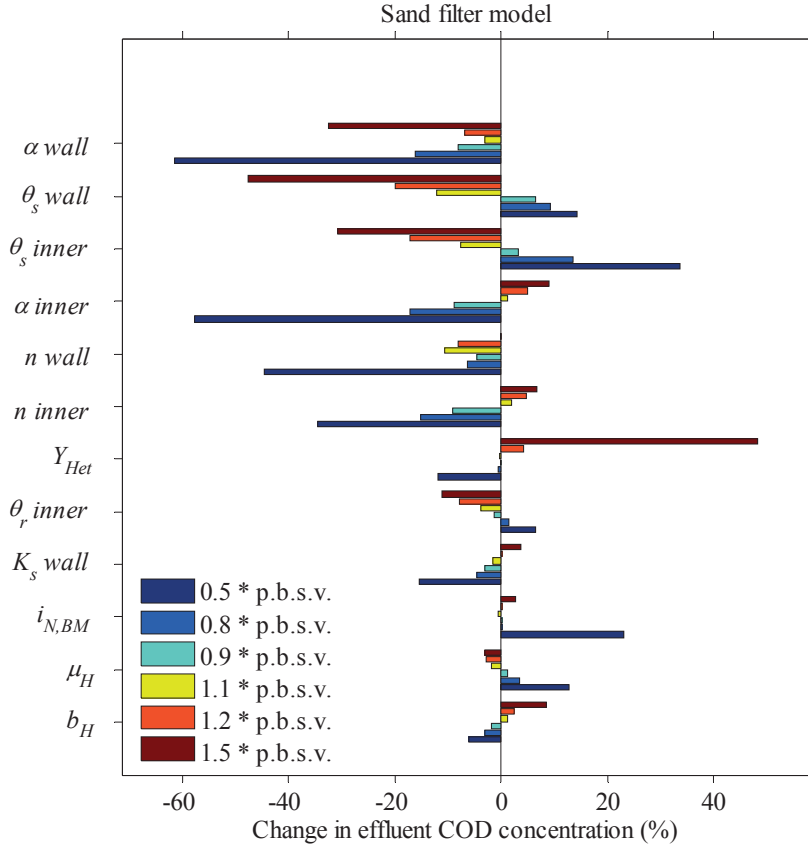

Figure 15. Simulated percentage change in effluent COD concentration for simulations with selected sand model parameters varied one at a time as 0.5, 0.8, 0.9, 1.1, 1.2 and 1.5 times the parameter base scenario value (p.b.s.v.). Selection based on when the mean of the absolute percentage changes of simulated effluent COD concentrations was larger than 3 % for a particular parameter (varied as 0.5, 0.8, 0.9, 1.1, 1.2 and 1.5 times its p.b.s.v.).

5 Discussion

5.1 Flow model results

The estimated parameters for the sand filter model greatly improved the fit (d = 0.99, E = 0.94), and the fit was further improved by adding the wall flow effects to a second sand filter model (d = 0.999, E = 0.996) compared with a model using a HYDRUS wetland module standard parameter set (d = 0.66, E = 0.18) (Table 4) (**Paper I**). Obtaining an increase in fit due to a higher degree of adjustment of the model was anticipated. The built-in inverse simulation function of HYDRUS, that was used to determine the flow parameters, has been applied successfully in previous studies (Dittmer *et al.*, 2005; Toscano *et al.*, 2009).

With this experience gained on calibrating the sand flow model, it was assumed that using the built-in inverse simulation function for parameter estimation was suitable also for modelling the bark and charcoal filters in (**Paper II**).

For the bark and charcoal filter models, the porosity was used as a fitting parameter even though it had previously been measured. The measured porosity was 0.73 for bark and 0.85 for charcoal (Dalahmeh *et al.*, 2012), in contrast to the estimated values of 0.41 and 0.14 respectively. The hydraulic properties of the filter material, such as the porosity, were measured before the filters were subjected to artificial greywater loadings. The difference might therefore be explained by compaction of the filter material during the experiments, mainly due to shrinking and swelling in the bark filter material and crushing of pellets for the charcoal filter.

Comparing simulated with measured cumulative effluent volume, all filter models performed well, with small NRMSE of 0.7-3.5% (Table 4), which demonstrates that HYDRUS is suitable for simulating water flow through sand as well as bark and charcoal filter media.

5.1.1 Flow model uncertainties and model deficiencies

There were a couple of suspected minor contributors to uncertainty and model incorrectness. For the charcoal flow model the inverse simulation for estimation of flow parameters failed, meaning that the simulation stopped without producing results, when the full one-day length data set was used as input (**Paper II**). The main suspected cause of this failure was the large number of data points in the objective function and/or uncertainty of the exact loading time.

When the function was run with a reduced number of data points, including only the first 400 minutes after the first loading, the parameter estimation was successful. When the estimated parameter set was tested on the full one-day length data-set with doubled HLR, the fit was good, demonstrating that the reduced objective function was sufficient for estimating the hydraulic parameters.

One model inaccuracy identified for the bark filter was swelling of the material not being incorporated in the model (**Paper II**). The swelling probably had an effect on porosity, being a function of water content. If it had been possible to include this aspect in the modelling with HYDRUS, the bark filter model might have produced simulated results with a better fit to measured values.

For all three filter types, the fact that evaporation in the experimental set-up was not completely prevented was neglected in the modelling. The amount of water lost due to evaporation is mainly dependent on upper surface area and should have been about the same for both hydraulic loadings (1 and 2 l day^{-1}). This means that evaporation should have had a larger effect on the observations made of the smaller loading of 1 l day^{-1} and this was the dataset used for estimation of parameters. The validation of the filter models with double flow, demonstrating good fit (Table 4), indicated that the parameter estimation was not disturbed to a considerable extent by the exclusion of evaporation.

5.1.2 Validation of flow models

The validation of the models supported the overall reliability of the estimated parameters since the calculated goodness-of-fit measures comparing simulated with observed cumulative effluent data indicated a close fit (E = 0.92 and d = 0.96, for all three filter types) (Table 4) (**Paper I** and **Paper II**). The validation hence indicated that the models were suitable for simulations of different HLR within the range tested (up to 1840 ml loadings).

Moriasi *et al.* (2012) established common guidelines for calibration and validation of hydrological models, including HYDRUS. Moriasi *et al.* (2012)

also stressed the need for calibration and validation of models before use in research or other applications. The recommended validation approach for most models, including HYDRUS, is split sample. The suggested performance evaluation for HYDRUS is demonstrating time series or statistical calculation of coefficient of determination and objective functions (Moriasi *et al.*, 2012). Using one data series for calibration and another for validation, as was done in this thesis, is arguably an even stronger evaluation than split sample. Following the recommendations of Ahnert *et al.* (2007), calculating *E* and *d* also provides a solid demonstration of the goodness-of-fit.

However, *E* has been shown by Willmott *et al.* (2012) to be a more well-behaved measure than *d* and they suggest a refined version of *d* to replace the earlier versions. This refined *d* was not included in the present thesis as it is monotonically and functionally related to *E*. The *d* as given here in its old form served the purpose of providing a basis for comparison with other, earlier work.

5.1.3 Wall flow effect in sand filter

Different degrees of calibration of the flow model for the sand filter were tested (**Paper I**). Estimated parameters (α and n) greatly improved the fit (d = 0.99, E = 0.94) and the fit was further improved by including wall flow effects (d = 0.999, E = 0.996) (Table 4). The sensitivity analysis also demonstrated that the hydraulic parameters of the outer wall layer had a large impact on the simulated effluent COD. However, increasing the number of fitting parameters from two to seven risks 'ill-posedness' of the inverse problem, as pointed out by Morvannou *et al.* (2013). Even though the model supported the occurrence of wall flow effects, both due to improved flow model fit (Table 4) and simulated BOD_5 in the effluent, wall flow effects were not confirmed to have occurred in the experimental set-up.

The estimated K_s for the outer wall layer (3720 cm h^{-1}) could, through the Hagen-Poiseuille equation, be interpreted as the wall layer having pores of 5 mm. In the experimental set-up, by visual inspection the pores next to the wall of the sand filter were most likely smaller than this. Furthermore, the distribution of uranin in the sand filters after adding a pulse of this fluorescent tracer displayed only moderate to low wall flow effects. After adding an NaCl tracer there was a rapid increase in EC in the sand filter effluent, which confirmed rapid transport of the greywater through the sand filters, but this could have been the result of either channel flow within the filter or wall effects (**Paper I**).

It was concluded that constructing an experimental set-up which isolates the wall layer for measurement of Q_s and K_s would reduce the number of fitting

parameters and allow in-depth study of wall flow effects. However, wall flow effects are most likely a problem that only occurs in laboratory-scale filters, in particular when using columns with small radius (**Paper I**).

To the best of my knowledge, no previous published study has simulated wall flow effects in filters. Simulation of wall flow effects could possibly also be viewed as simulation of preferential flow, which could be of interest in other applications, such as simulation of a partially clogged filter.

Wall flow effects for the bark and the charcoal filters (**Paper II**) were not considered. The swelling of the bark chips during loading made the material press against the column walls and hence prevented any faster flow from happening there. For the charcoal filter, there was only a small amount of easily biodegradable organic material in the filter effluent. This indicated that the greywater did not bypass the filter to a great extent through wall flow effects or similar. In the charcoal filter, the charcoal pellets were most likely crushed against the wall during packing and continuous loading, thus preventing large pores from appearing next to the wall.

5.1.4 Verification of the flow models

For each simulation made, the mass balance was used as a control. If the mass balance is shown as close to zero, no water has been created or lost in the simulation, indicating that there are no numerical errors. There are also certain limits to values that can be enforced within HYDRUS, such as the soluble oxygen amount. If such a limit has been enforced and the simulation overrides the limit, it is an indication of numerical error. Before analysing simulation results, all simulated components were checked for discrepancies, such as values reaching infinity, which would be evidence of numerical error.

Since HYDRUS is a widely used commercial software, it was assumed that the developers ensure the code is free from bugs and regularly work on finding and solving numerical issues related to the coding.

When estimating flow parameters, different initial values for the estimated parameters were tested in this thesis. For all initial values tested, the inverse function converged to the same parameter set, or did not converge at all. This indicates that there was uniqueness to the estimated flow parameters.

5.2 Modelling biomass

One of the major changes made in model parameter values of HYDRUS CW2D was the calibration of lysis rate constant (b_H) and maximum aerobic growth rate (μ_H). This was done in order to curb the excessive continuous

growth of biomass that occurred in the simulated filters when using default values (both **Paper I** and **Paper II**).

XH was set to match potential respiration rate measurements, using the same calibration procedure for the sand filter model (**Paper I**) as for the bark and charcoal filter models (**Paper II**). The method of calibration was according to the procedures of Langergraber *et al.* (2007), who presented formulae to estimate the simulated heterotrophic microbial biomass from different measurements of microbial activity of subsurface vertical flow constructed wetlands treating municipal wastewater. The measurements were taken from three different methods to quantify biomass, including substrate induced respiration (SIR), ATP measurement and fumigation-extraction (Tietz *et al.*, 2007). The study demonstrated large differences (up to 1669 µg COD g sand^{-1}) in calculated biomass COD depending on the method used for the calculation (Langergraber *et al.*, 2007). Petitjean *et al.* (2012) have also used calibration of lysis rate constant (b_H) as a fitting parameter for simulating biomass in vertical flow with coarse sand (0-4 mm) as filter material.

As noted by Langergraber *et al.* (2007), it is difficult to obtain a parameter set that produces a long-term simulation where biomass amounts correspond to observed values for all depths of the filter. When constant biomass was simulated for the lower part of the sand filter (20-60 cm depth), the biomass grew excessively in the top layer (**Paper I**). When parameters were chosen to curb the excessive growth in the top layer, the biomass at lower layers died off. The same was noted for the bark and charcoal filter (**Paper II**). The simulated die-off in the bottom of the filters, in contrast to the growth demonstrated by the measurements, might be explained by the fact that in the experiment, the outlet allowed air to enter the filter. This aerated the bottom of the filter and possibly promoted microbial growth there. The air flow should perhaps have been prevented *e.g.* by installing an air lock.

The heterotrophic biomass in the sand filter material comprised amounts corresponding to 236 µg COD g sand^{-1}, which was small compared with the maximum of 5100 µg COD g sand^{-1} observed by Langergraber *et al.* (2007) but closer to the 200-1700 µg COD g sand^{-1} reported by Pell *et al.* (1990) and Campos *et al.* (2002). Campos *et al.* (2002) studied slow sand filtration (filter sand with 0.1-0.3 mm effective particle size) for treatment of river water. They concluded that small populations of microorganisms were sufficient for river water purification and observed no major advantages of increased concentration of biomass. The simulated growth in **Papers I** and **II**, as well as the measurements and several other studies, show that biomass is most dense in the top layer of the filters (Pell *et al.* 1990; Campos *et al*., 2002; Dalahmeh *et al.*, 2014a; Tietz *et al.*, 2007).

For the sand filter model including wall flow effects, the simulated biomass occurred in higher concentrations in the wall layer than in the inner material (**Paper I**). Thus, the model indicated that microbial growth is promoted in the wall layer, where the measurements in the experimental filter were actually taken. This suggests that measurements taken within the filter would have demonstrated smaller values. Taking measurements from the centre of a filter material is almost impossible, however, without causing major disturbance to the continued operation of the filter.

The bark filter model overestimated *XH* in the filter top layer and at 20 cm depth (2950 and 1950 µg COD g material^{-1} compared with observed 1495 ± 465 and 847 ± 236 µg COD g material^{-1}) (**Paper II**). It was not possible to manually balance the parameters b_H and μ_H so that the model would simulate *XH* corresponding to observed amounts for all depths of the bark filter. Since the observations clearly demonstrated large amounts of biomass throughout the bark filter depths, the model with overestimated biomass at the top layers but viable biomass in the lower filter depth was chosen over having adjusted biomass at the top of the filter but close to zero amounts in the lower part of the filter.

It might have been possible to achieve a balance if an add-on for estimating the biological parameters had been developed. The HYDRUS wetland module could be improved by adding restrictions to biomass growth, *e.g.* adding consideration of limited growth space and actual access to nutrients.

The charcoal filter model, on the other hand, simulated *XH* close to observed amounts for all depths (525, 400, 260 and 115 µg COD g material^{-1} compared with observed 478 ± 161, 335 ± 142, 210 ± 161 and 141 ± 139 µg COD g material^{-1}) over the five-day time span (**Paper II**).

It was demonstrated by simulation that *XH* increases when the bark and the charcoal filters are subjected to higher OLR, which enabled the filters to maintain a high COD removal (70-90%) even while subjected to OLR of 28 g BOD_5 m^{-2} day (**Paper II**). This was consistent with measured COD removal (68-95%). The bark and charcoal filter models simulated amounts of *XH* in the filters (12-14600 µg COD g material^{-1}) quite larger than the 3-5100 µg COD g sand^{-1} observed by Tietz *et al.* (2007) and the 200-1700 µg COD g sand^{-1} reported by Pell *et al.* (1990) and Campos *et al.* (2002).

5.3 Simulation of organic matter removal

The measured concentration of effluent BOD_5 (108 ± 57 mg COD l^{-1}) compared well with the simulated effluent *CR* by the sand filter model that included wall flow effects (139 mg COD l^{-1}) (**Paper I**). The concentration of

effluent total COD was slightly overestimated by that model, which gave 338 mg COD l^{-1} compared with the measured 245 ± 106 mg COD l^{-1} (Table 6). The over-estimation of pollutants in the effluent indicated that the simulated wall flow effects were exaggerated (**Paper I**).

It was demonstrated for the sand filter model that the effect of increased heterotrophic biomass (*XH*) produced a noticeable effect on filter effluent COD concentration (300 mg COD l^{-1} compared with 337 mg COD l^{-1}). This indicated that the average biomass measurements might have underestimated the actual concentrations and that the model could benefit substantially from increased accuracy and precision in determining *XH* (**Paper I**). This could be true also for the bark and charcoal filter models.

The simulated bark filter effluent concentration of COD (92 mg l^{-1}) was less than the measured value (200 ± 7 mg l^{-1}) (**Paper II**). The removal of COD in Run 1, 2 and 5 was simulated as 90, 88 and 90 % respectively, which was 13-20 percentage points above observed (75 ± 8, 68 ± 11 and 81 ± 7 % respectively). This difference between simulated and observed data could partly be explained by release of organic matter from the bark material itself. Dalahmeh *et al.* (2014) observed that a bark filter continuously fed tap water (1 l day^{-1}), released 95 ± 14 mg COD l^{-1} (n = 1) at start-up and 55 ± 8 mg COD l^{-1} (n = 1) after 85 days. This was similar to the observations by Ribé *et al.* (2009), who studied leaching of contaminants from untreated pine bark and noted a dissolved organic carbon concentration in the effluent of 69 mg l^{-1}. Genç-Fuhrman *et al*. (2007), who used bark filters for testing removal of heavy metals from stormwater, also noted release of organic material to the effluent from the material.

Subtracting 75 mg COD l^{-1} from the observed bark filter effluent and recalculating the removal would yield 86, 81, 78 and 83 % removal of COD in Run 0, 1, 2 and 5 respectively. This gives a closer fit to the observed values (77 ± 4, 75 ± 8, 68 ± 11 and 81 ± 7 %, respectively) than the nonadjusted data (90, 90, 88 and 90 %, respectively) (**Paper II**).

The charcoal filter model simulated effluent COD as 57 mg l^{-1}, which compared well to the observed, 48 ± 11 mg l^{-1}. In Run 0 and Run 1, which were the most similar loading regimes, the simulated COD removal (94 and 91 %, respectively) compared well to the observed values (95 ± 2 and 89 ± 11 %, respectively). However, simulated COD removal for Run 2 (70 %) and Run 5 (72 %) was low compared with observed (90 ± 7 and 84 ± 4 %) (**Paper II**).

Rizzo *et al.* (2014) modelled the response of laboratory horizontal flow constructed wetlands to unsteady organic loads with the HYDRUS wetland module, using the setting "CWM1". They used concentrated synthetic wastewater to represent municipal wastewater, which was diluted before being

loaded onto the experimental filters according to a schedule to mimic weekly variations. In their simulations, the average overall removal efficiency of simulated COD (68%) was close to the value observed in experiments (67%). The simulated response to unsteady loads at daily scale had a mean error of 20% when compared with observations. The fit of simulated to observed organic matter removal demonstrated by Rizzo *et al.* (2014) is comparable to the fit achieved here for the bark, charcoal and sand filter models.

5.3.1 Specifying the COD fractionation of the models

Different fractionation of model COD was used for the sand filter model (**Paper I**) than for the bark and charcoal filter models (**Paper II**). For the sand filter model, the fractionation was based on an assumption that the fractionation of *CR*, *CS* and *CI* could be related to the ratio of influent BOD_5 to COD. This assumption was justified to some extent by the demonstration of good fit of simulated outgoing concentrations of COD to observations. However, even though a relationship between *CR*, *CS* and *CI* fractionation to the influent BOD_5:COD ratio is likely, it should be confirmed through statistical measures. This could be done by having a series of filters fed with artificial greywater with different BOD_5 and COD ratios. The CI fraction could be determined as the difference in final COD and BOD, which would be correct for the model's definition of *CI* as inert material. The fractionation of *CS* and *CR* should then be fitted to obtain a good match between simulated and observed effluent concentration of COD. The relationship between the fractions of *CS* and *CR* and influent BOD_5 and COD ratios could then be determined through linear regression. To the best of my knowledge, this has not been done in any published study.

For the bark and charcoal filter models, the same fractionation as was done for the sand filter model was tested, but the model fit of simulated to observed data was not good. Therefore, another method, repeatedly used in previous studies (Dittmer *et al.*, 2005; Henrichs *et al.*, 2007; Langergraber *et al.*, 2007; Toscano *et al.*, 2009), was used (**Paper II**). This method, which assumes a relationship between the model's *CR*, *CS* and *CI* fractions and observed effluent COD concentration, is a rule of thumb. There is currently a lack of research on more well-founded methods to determine the *CR*, *CS* and *CI* fractions in the HYDRUS wetland module.

The HYDRUS wetland module is based on the Activated Sludge Model (ASM) (Henze *et al.* 2000), which also uses a fractionation of dissolved COD in terms of readily biodegradable substrate (S_F), fermentation products (S_A) and inert, non-biodegradable organics (S_I). The ASM further incorporates two fractions of particulate COD; inert non-biodegradable organics (X_I) and slowly

biodegradable substrate (X_S). Henze *et al.* (2000) suggest values of these components for simulating activated sludge treatment of typical wastewater (primary effluent, total COD concentration of 260 g COD m^{-3}, total nitrogen concentration of 25 g m^{-3} and total phosphorus concentration of 6 g m^{-3}). However, the same fractionation is not suitable for use for the HYDRUS wetland module's CW2D setting, since the particulate components of organic matter (X_I and X_S) are not included. Furthermore, even though the HYDRUS wetland module is based on the ASM, inherently different treatment systems are considered (constructed wetlands versus the activated sludge process of municipal treatment plants).

In conclusion, two different methods were explored to determine the *CR*, *CS* and *CI* fractions. The method used for the sand filter model points towards the possibility that the model *CR*, *CS* and *CI* fractions can be related to observed influent BOD_5 and COD concentrations (**Paper I**), while the method used for the bark and charcoal filter models (**Paper II**) applies a well-known rule of thumb to the new context of bark and charcoal filter media. As described above, it might be possible to further develop the method used for the sand filter (**Paper I**).

5.4 Discussion of the sensitivity analysis

Langergraber (2001) performed a sensitivity analysis (SA) of CW2D that included 53 parameters, with default values for parameters set as start values. In this SA, each parameter was increased or decreased by 10% while all other parameters were kept constant and the results were then compared with the start run with all parameters set to default values. The simulation time span was set to five days and only results from day 5 were used.

Langergraber (2001) concluded that all material parameters, except the residual water content (θ_r), are among the parameters with the strongest influence on effluent concentrations. It is therefore essential to calibrate the hydraulic parameters in order to get a representative model. The results from the NRSA performed in this thesis agree with this conclusion, with the exception that the residual water content parameter demonstrated a notable influence on effluent COD concentrations for all filter models. The filter models could possibly have benefited if the residual water content of the filter materials had been determined experimentally and provided the model with other values than the default value used.

Other parameters with a strong influence on effluent concentrations according to Langergraber (2001) were the oxygen re-aeration rate ($k_{aer,O2}$), the heterotrophic yield coefficient (Y_H), the heterotrophic lysis rate (b_H) and the

parameters for hydrolysis (K_h and K_X). This was also demonstrated to some extent in the SA in this thesis, with the exception that none of the filter models tested here was sensitive to the oxygen re-aeration rate. Furthermore, only the bark and charcoal filter models were sensitive to K_h and only the charcoal filter model was sensitive to K_X.

The charcoal filter model displayed the overall largest change in effluent COD concentrations (+1121% for 1.5 times the heterotrophic yield coefficient) compared with the bark model (+122% for 0.5 times α) and the sand model (-61% for 0.5 times α of the wall material). The parameter value of the heterotrophic yield coefficient, causing an unrealistic change in the charcoal model effluent COD concentration but not in the bark or sand models, had the same base scenario value in each filter model. This result demonstrates that the heterotrophic yield coefficient is a highly non-linear parameter. On decreasing the porosity (θ_s) to 0.5 times the base scenario value, another somewhat unrealistic response in the charcoal model effluent COD appeared (+ 484%). The charcoal filter model had a porosity of 0.14 in the base scenario, which is quite low already, so it is therefore not very surprising that halving this value would cause model discrepancy.

For the sand filter model, the NRSA demonstrated that the material parameters of the wall layer (α, θ_s, n and K_s) had large impacts on the effluent COD concentration. This suggests that heterogeneity within the filter filling will influence the effluent concentration of COD.

The parameters were varied as 0.5, 0.8, 0.9, 1.1, 1.2 and 1.5 times the base scenario value, as in the study by Ketema and Langergraber (2015), who used parameter perturbation of ± 5, ± 10, ± 15 and ± 20 % from the base value to study CLARA, a simplified modelling tool for estimating the life cycle cost of water supply systems. Ketema and Langergraber (2015) also used a derivative-based method for their SA, which consisted of using a sensitivity coefficient calculated from the percentage change in output divided by the percentage change in the parameter. This was different from the positive (or negative) percentage change compared with the base scenario effluent COD as suggested by Frey & Patil (2002), which was applied in this thesis.

The reason why each model showed sensitivity of varying degrees to different parameters is most likely because the HYDRUS wetland module is non-linear. Nominal sensitivity analysis is best suited for linear models and Frey and Patil (2002) suggest that for a non-linear model, the sensitivity of the output may depend strongly on interactions between several parameters. The sensitivity analysis could therefore be extended to include the Response Surface Method (RSM) to evaluate the relationship between the model output of interest and one or more explanatory parameters. For this method, it is an

advantage to use the results from the nominal sensitivity analysis to limit the number of parameters to include only the most important. A Monte Carlo simulation strategy can then be employed to generate a large number of various combinations of parameter sets, which are simulated for recording the output. A statistical method is then applied to the results, for example analysis of variance (ANOVA), which will give a 'model of the model' but with the advantage of being simpler than the original model.

Proceeding with RSM to further study the interactions of the HYDRUS wetland module parameters is unlikely to be useful, however. Having a deterministic model is often preferable over a statistical model because of the stronger connection of a deterministic model to reality. Parameters of a deterministic model can be directly measured, whereas parameters of a statistical model typically need to be estimated from large datasets. Furthermore, the nominal sensitivity analysis suffices to give an overview of the most relevant parameters for model calibration.

The NRSA in this thesis showed that six parameters, fraction of *CI* generated in biomass lysis, yield coefficient for *XH*, hydrolysis rate constant, saturation/inhibition coefficient for hydrolysis, maximum aerobic growth rate and the N content of biomass influenced the effluent COD concentration. Further studies are needed to test whether the default values for these parameters are representative for all vertical flow filters, in particular when alternative filter media to sand are used. It is possible that the models can be made more representative of reality by tuning these parameters to other, experimentally determined values.

6 Outlook

6.1.1 Effluent nitrogen and phosphorus concentrations

Although nitrogen and phosphorus compounds were not targeted within the aims of this thesis, they still had to be specified in the simulated influent in order for the models to run properly. With the availability of observed nitrogen and phosphorus concentrations, simulated results for nitrogen and phosphorous were checked so that no major discrepancies went un noticed. In order to limit the scope of the thesis, the filter models were not calibrated to perform with great accuracy for nitrogen and phosphorus simulation. However, the results are briefly described here as the basis for potential continued research on simulating these compounds.

Nitrogen is simulated in the HYDRUS wetland module as nitrate (*NO3N*), nitrite (*NO2N*) and ammonium (*NH4N*) and total nitrogen is calculated as *NO3N* + *NO2N* + *NH4N* + nitrogen content of outgoing COD. Nitrite is not shown here, however, because it was close to zero in both observed and simulated results. Phosphorus is simulated as inorganic phosphorus (*IP*) and total phosphorus (*TP*), which is calculated as *IP* + phosphorus content of outgoing COD.

Run 0 of the bark, charcoal and sand models all simulated nitrogen to be present in the filter effluent (mean *TN* effluent concentration of 70, 35 and 48 mg l^{-1} respectively) whereas measured mean *TN* effluent concentrations were 64 ± 7, 1 ± 0 and 72 ± 10 mg l^{-1} respectively (Table 8).

The models also simulated phosphorus to be present in the filter effluents for Run 0 (mean *TP* effluent concentration of 2.7, 1.8 and 3.2, respectively) whereas measured mean *TP* effluent concentrations were close to zero for the bark and charcoal filters and 0.9 ± 0.2 mg l^{-1} for the sand filter (Table 8).

Table 8. *Measured mean filter influent and effluent concentrations of pollutants (Dalahmeh et al. 2012) and the corresponding simulated values. For abbreviations see text*

Parameter	Sim. infl. conc. (mg l^{-1})	Obs. filter effl. conc. (mg l^{-1})			n	Sim. filter effl. conc. (mg l^{-1})		
		Bark	Charcoal	Sand		Bark	Char.	Sand
NO3N	1	51 ± 7	0 ± 0	57 ± 7	10	60	29	10
NH4N	0.5	0 ± 0	0 ± 0	4.8 ± 0.4	10	5	0	8
TN	76	64 ± 7	1 ± 0	72 ± 10	4	70	35	48
IP	2.1	0 ± 0	0 ± 0	0.4 ± 0.1	10	2.5	1.7	2.4
TP	4.2	0.1 ± 0	0.3 ± 0.1	0.9 ± 0.2	4	2.7	1.8	3.2

The simulated *TN* removal compared well with the observed for the bark model in loading regimes Run 0 and Run 1 and for the charcoal model in Run 1 and Run 2. Simulated *TP* removal compared well with the observed value only in Run 5 for both bark and charcoal filter models (Figure 16).

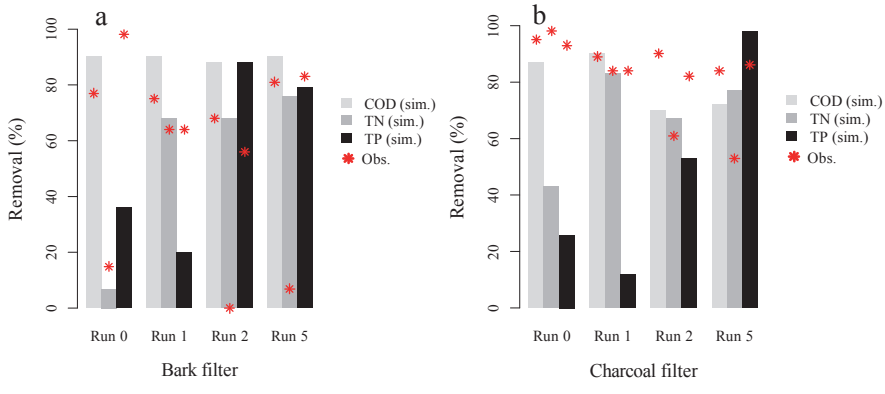

Figure 16. Simulated and observed (*) removal of chemical oxygen demand (COD), total nitrogen (*TN*) and total phosphorous (*TP*) at different loading regimes: Run 0: HLR = 32 l m^{-2} day^{-1}, OLR = 14 g BOD_5 m^{-2} day^{-1}; Run 1: HLR = 32 l m^{-2} day^{-1}, OLR = 13-16 g BOD_5 m^{-2} day^{-1}; Run 2: HLR = 64 l m^{-2} day^{-1}, OLR = 14 g BOD_5 m^{-2} day^{-1}; Run 5: HLR = 32 l m^{-2} day^{-1}; OLR = 28 g BOD_5 m^{-2} day^{-1} using *(a)* the bark filter model and *(b)* the charcoal filter model.

These results indicate that the simulation of nitrogen, especially with the charcoal filter model but to some extent also with the sand filter model, was incomplete and the filter functions were not completely represented by the models. Being able to model nitrogen release from these types of filters is important in different aspects. Dalahmeh *et al.* (2012) commented on the suitability of using treated greywater for irrigation and pointed out that nitrogen remaining in the water after treatment is an asset. Modelling nitrogen transport in the filters could therefore be used to develop a filter design with the goal of preserving the nitrogen while treating organic matter. Dalahmeh *et*

al. (2012) also suggested drip-irrigation to minimise the risk of nitrogen-rich irrigation water polluting the ground water.

The issue of nitrogen-rich effluents from onsite wastewater treatment systems affecting local water quality makes modelling nitrogen dynamics interesting from another perspective. Kirkley *et al.* (2007) raised the problematic situation of the urban front-range corridor of Colorado, where the increasing use of onsite wastewater treatment systems is possibly posing a threat to the local aquifers used for drinking water. Kirkley *et al.* (2007) used HYDRUS 1D to simulate nitrate concentrations released from onsite wastewater treatment systems reaching groundwater. They identified the denitrification rate coefficient as the most important input parameter, because reasonable values for this parameter range over three orders of magnitude and at the same time the model is highly sensitive to its value. Their conclusion was that for reasonable rates at the lower end of the reported range, the simulations showed that nitrate reached the groundwater in concentrations above the regulatory limits.

Simulated phosphorus effluent concentrations were much higher than observed values for all filter types tested in this thesis, especially the bark and charcoal filters. The mechanism of an infiltration-type wastewater treatment system for removing phosphorus is very limited. Phosphorus, unlike nitrogen or organic matter, cannot exit the system through entering the gas phase and only a minimal amount of phosphorus is embedded in the biomass as a macronutrient for micoorganisms.

However, it is possible for phosphorus to adsorb to the filter material. Xiuwen *et al.* (2014) studied the adsorption properties of 10 potential constructed wetland filter materials: gravel, volcanic gravel, crushed stone, broken bricks, bio-ceramic, anthracite, blast furnace slag, activated carbon, sand and zeolite. They found that both Freundlich and Langmuir isotherms could adequately predict the adsorption process. They ranked activated carbon as having higher maximum adsorption capacity than sand or gravel, but in their conclusions they recommend bio-ceramics or anthracite as materials for phosphorus removal.

The bark filter also demonstrated low concentrations of total phosphorus in the effluent (0.1 mg l^{-1}) compared with the influent (4.2 mg l^{-1}), indicating efficient phosphorus removal. Tshabalala *et al.* (2004) studied cationized milled pine bark as an adsorbent for orthophosphate anions and concluded from batch adsorption experiments that this material has a maximum adsorption capacity of approximately 12.65 mg phosphate g^{-1}. This is comparable with that of other well-known phosphorus sorbents, *e.g.* Cucarella and Renman (2009) reports the phosphorus adsorption capacity of gravel (3-10

mm diameter), sand (0-5 mm diameter) and Filtralite (0-2 mm diameter) to be 0.03-0.05, 0.13-0.29 and 1.39-2.21 mg phosphate g^{-1} respectively. Those authors found the highest phosphorus adsorption capacity for blast furnace slag, fly ash and red mud (44.25, 63.22 and 113.87 mg phosphate g^{-1}, respectively). However, there appears to be a lack of research on the adsorption of phosphorus to raw bark material. There is thus a need for further studies to conclude whether adsorption of phosphorus is the reason for the low phosphorus concentrations observed in the bark filter effluent in this thesis. This aspect could then be incorporated into the bark filter model with the use of experimental data to determine relevant adsorption parameters.

Furthermore, there is a possible need to determine how long the bark filter can operate until depletion of adsorption sites is reached. If adsorption of phosphorus to the bark filter material is unwanted because the filter effluent is to be used for irrigation, Cucarella and Renman (2009) mention several parameters affecting adsorption systems, such as pH, contact time and temperature, which could be adjusted to achieve optimal filter performance. Computer modelling of the filter could be used as a guiding tool to determine these parameters.

6.1.2 Possible filter design developments

There are many possibilities to use the computer modelling results in this thesis for improving filter design, *e.g.*:

- Length of filter columns. A series of simulations testing filter column length could identify the optimum length in a number of case studies. Suitable case studies could be to develop adequate treatment performance for lowest possible cost (*e.g.* using a minimum of space and filter material), best treatment performance possible for high protection of certain areas or ability to withstand shock loads.
- Different loading operations. The performance of the filters if the loadings were distributed in smaller portions over the day or operated with continuous drip. This could be combined with testing shock loads to see if the filter better withstands shock loads using certain loading operations.
- Particle size. How different particle sizes influence treatment performance and whether different particle sizes are suitable depending on material.
- Filter clogging. To evaluate the clogging process using the model, one could run a series of simulations where the porosity was reduced step-wise. This could help predict the reduction in pore size at which the filter material needs to be cleaned/exchanged. This could be tested in

relation to length of filter column and/or particle size of filter media to demonstrate the sensitivity of these filter characteristics to clogging.

- Using layers of different materials in the same filter column or having a series of filter columns (*e.g*. a charcoal filter column as a polishing step for the bark filter effluent) and examining whether different filter materials contribute meaningfully to the treatment effect when combined in layers.

7 Conclusions

- Estimation of two soil hydraulic parameters, the inverse air entry value and the pore connectivity parameter, for the sand filter model greatly improved the fit of simulated compared with observed cumulative effluent data. The fit was further improved by increasing the number of estimated parameters to seven by adding a wall layer to the transport domain of the model with all parameters estimated, which is believed to correspond to wall flow effects.
- Measured substrate-induced respiration rate can be used to estimate the amount of biomass in bark, charcoal and sand vertical flow filters. Using these data, the filter model biomass can be calibrated to correspond to estimated mean amounts of biomass and this will lead to a more representative model than using standard parameters alone.
- More measurements are needed to determine long-term trends in the biomass in bark, charcoal and sand vertical flow filters. The HYDRUS wetland module could also be improved by allowing limitation of microbial growth and adding the possibility to simulate clogging.
- Organic matter degradation in vertical flow bark, charcoal and sand filters can be simulated using filter models developed in the HYDRUS wetland module. When simulating regimes with higher hydraulic and organic loading rates with the bark and charcoal filter models, the simulated results demonstrated a larger deviation from experimental observations but were in an acceptable range of 1-20 percentage points with regard to filter COD removal (%).
- Possible uses of the filter models to develop filter design include simulating and evaluating filter column length, particle size, loading operation and layering of different materials in the same filter.

References

Anderson, J. P. E. and Domsch, K. H. (1977). A physiological method for the quantitative measurement of microbial biomass in soils. *Soil Biology & Biochemistry,* 10, 215-221.

Ahnert, M., Blumensaat, F., Langergraber, G., Alex, J., Woerner, D., Frehmann, T., Halft, N., Hobus, I., Plattes, M., Spering, V. and Winkler, S. (2007). Goodness-of-fit measures for numerical modelling in urban water management – a review to support practical applications. In: IWA (eds.): *Proceedings of the 10th IWA Specialised Conference on "Design, Operation and Economics of Large Wastewater Treatment Plants"*, 9-13 September 2007, Vienna, Austria, 69-72.

Argun, M. E., Dursun, S. and Karatas, M. (2009). Removal of Cd(II), Pb(II), Cu(II) and Ni(II) from water using modified pine bark. *Desalination*, 249 (2), 519-527.

Brooks, R. H. and A. T. Corey (1964). Hydraulic properties of porous media, *Hydrol. Paper No. 3*, Colorado State University, Fort Collins.

Brovelli, A., Malaguerra, F. and Barry, D.A. (2009). Bioclogging in porous media: Model development and sensitivity to initial conditions. *Environmental Modelling & Software*, 24, 611-626.

Campos, L. C., Su, M. F. J., Graham, N. J. D. and Smith, S.R. (2002). Biomass development in slow sand filters. *Water research*, 36, 4543-4551.

Calaway, W. T. (1957). Intermittent Sand Filters and Their Biology. *Sewage and Industrial Waste*, 29 (1), 1-5.

Corbould, C. (Future Directions International) 2013. Feeding the cities: Is urban agriculture the future of food security? *Future Directions International*, Australia.

Cucarella, V. and Renman, G. (2009). Phosphorus Sorption Capacity of Filter Materials Used for On-site Wastewater Treatment Determined in Batch Experiments - A Comparative Study. *Journal of Environmental Quality*, 38, 381-392.

Cullen, A. C. and Frey, H. C. (1999). Probalistic Techniques in Exposure Assessment. *Springer Publishing*, ISBN 978-0-306-45956-6, New York, US.

Curtis, T. P. and Sloan, W. T. (2005). Exploring Microbial Diversity - A Vast Below. *Science*, 309 (5739), 1331-1333.

Dalahmeh, S., Pell, M., Vinnerås, B., Hylander, L., Öborn, I. and Jönsson, H. (2012). Efficiency of Bark, Activated Charcoal, Foam and Sand Filters in Reducing Pollutants from Greywater. *Water Air Soil Pollut.* Volume 223, p. 3657-3671.

Dalahmeh, S.S., Jönsson, H., Hylander, L.D., Nan, H. and Pell, M. (2014a). Dynamics and functions of bacterial communities in bark, charcoal and sand filters treating greyawter. *Water Research*, 54, 21-32.

Dalahmeh, S., Pell, M., Hylander, L., D., Lalander, C., Vinnerås, B., Jönsson, H. (2014b). Effects of changing hydraulic and organic loading rates on pollutant redcution in bark, charcoal and sand filters treating greywater. *Journal of Environmental Management*, 132, 338-345.

Dittmer, U., Meyer, D. and Langergraber, G. (2005). Simulation of a subsurface vertical flow constructed wetland for CSO treatment. *Water Science and Technology*, 51 (9), 225-232.

Donner, E., Eriksson, E., Revitt, D. M., Scholes, L., Lutzhoft, H. and Ledin, A. (2010). Presence and fate of priority substances in domestic greywater treatment and reuse systems. Science of the Total Environment, 408, 2444-2451

Droste, R. L. (1997). Theory and Practice of Water and Wastewater Treatment. *John Wiley and Sons,* Canada.

Durner, W. (1994). Hydraulic conductivity estimation for soils with heterogeneous pore structure, Water Resources Research, 32 (9), 211-223.

Eriksson, E., Auffarth, K., Henze, M. and Ledin, A. (2002). Characteristics of grey wastewater, *Urban Water*, 4, 85-104

Frigg, R. and Reiss, J. (2007). The philosophy of simulation: Hot new issues or same old stew. *Synthese*, 169, 593–613.

Frey H. C. and Patil, S. R. (2002). Identification and Review of Sensitivity Analysis Methods. *Risk Analysis*, 22 (3), 553-578.

Genç-Fuhrman, H., Mikkelsen, P. S. and Ledin, A. (2007). Simultaneous removal of As, Cd, Cr, Cu, Ni and Zn from stormwater: Experimental comparison of 11 different sorbents. *Water Research*, 41, 591-602.

Giraldi, D., de'Michieli Vitturi, M. and Iannelli, R. (2008). FITOVERT: a dynamic numerical model of subsurface vertical flow constructed wetlands. *Proceedings of the "International Symposium on Sanitary and Environment (SIDISA.08)"*, Florence, Italy.

Guo, W. and Langevin, C. D. (2002). User's guide to SEAWAT: a computer program for simulation of three-dimensional variable-density ground-water flow. U.S. geological survey techniques of water-resources investigations (2002) Book 6, USA.

Henrichs, M., Langergraber, G. and Uhl, M. (2007). Modelling of organic matter degradation in constructed wetlands for treatment of combined sewer overflow. *Science of the total environment,* 380, 196-209.

Henze, M., Grady, L. C. P., Gujer, W., Marais, G. V. R., Matsuo, T. (1987). A general model for single-sludge wastewater treatment systems. *Water Research*, 21(5), 505-515.

Henze, M., Gujer, W., Mino, T., van Loosdrecht, M. (2000). Activated sludge models ASM1, ASM2, ASM2d and ASM3. ISBN: 1-900222-24-8. IWA Publishing, UK.

Herrmann, I., Hedström, A., Viklander, M., Jourak, A., Lundström, T., S. and Gustafsson, J. (2013). Modeling phosphate transport and removal in a compact bed filled with a mineral-based sorbent for domestic wastewater treatment. *Journal of Contaminant Hydrology*, 154, 70-77.

Humphreys, P. (2004). Extending Ourselves: Computational Science, Empiricism, and Scientific Method, ISBN: 978-0-19-531329-1. Oxford University Press (OUP), USA.

Heatwole, K. K. and McCray, J. E. (2007). Modeling potential vadose-zone transport of nitrogen from onsite wastewater systems at the development svale. *Journal of Contaminant Hydrology*, 91, 184-201.

Karlsson, S. 2012. *Modeling of bark-, sand- and activated carbon filters for treatment of greywater*. Msc. thesis. Uppsala: Swedish University of Agricultural Sciences.

Ketema, A. B. and Langergraber, G. (2015). Sensitivity analysis for water supply input paramaters pf the CLARA simplified planning tool using three complementary methods. *Journal of Water Supply: Research and Technology - AQUA*, in press.

Kosugi K. (1996). Lognormal distribution model for unsaturated soil hydraulic properties, *Water Resources Research*, 32 (9), 2697-2703.

Kristiansen, R. (1981). Sand-Filter Trenches for Purification of Septic Tank Effluent: III. The Mircoflora. *Journal of Environmental Quality*, 10, 361-364.

Langergraber, G. (2001). Development of a Simulation Tool for Subsurface Flow Constructed Wetlands. Doctoral thesis, Institut für Wasservorsorge, Universität für Bodenkultur, Wien.

Langergraber, G., Tietz, A. and Haberl, R. (2007). Comparison of measured and simulated distribution of microbial biomass in subsurface vertical flow constructed wetlands. *Water Science and Technology*, 56(3), 233-240.

Langergraber, G. and Šimůnek, J. (2012). Reactive Transport Modeling of Subsurface Flow Constructed Wetlands Using the HYDRUS Wetland Module. *Vadose Zone Journal*, 11 (2) Special Issue "Reactive Transport Modeling", doi:10.2136/vzj2011.0104.

Lens, P. N., Vochten, P. M., Speleers, L. and Verstraete, W. H. (1994). Direct treatment of domestic wastewater by percolation over peat, bark and woodchips. *Water Research*, 28 (1), p. 17-26.

Maimon, A., Tal, A. Friedler, E. and Gross, A. (2010). Safe on-site reuse of greywater for irrigation - a critical review of current guidelines. *Environmental Science and Technology*, 44 (9), 3213-3220.

Mao, X., Prommer, H., Barry, D. A., Langevin, C., D., Panteleit, B. and Li, L. (2006). Three dimensional model for multi-component reactive transport with variable density groundwater flow. *Environmental Modelling & Software*, 21 (5), 615–628.

Morgan, M. G., Henrion, M. and Small, M. (1992). Uncertainty: A Guide to Dealing with Uncertainty in Quantitative Risk and Policy Analysis. *Cambridge University Press*. Cambridge, NY. ISBN: 978-0521427449.

Moriasi, D. N., Wilson, B. N., Douglas-Mankin, K. R., Arnold, J. G., Gowda, P. H. (2012). Hydrologic and Water Quality Models: Use, Calibration and Validation. *American Society of Agricultural and Biological Engineers,* 55(4), 1241-1247.

Nash, J. E. and Sutcliffe, J. V. (1970). River flow forecasting through conceptual models part I – A discussion of principles. *Journal of Hydrology*, 10(3), 282.

Oreskes, N., Shrader-Frechette, K. and Belitz, K. (1994). Verification, Validation and Confirmation of Numerical Models in the Earth Sciences. *Science*, 263 (5147), 641–646.

Oberkampf, W., L. and Roy, C., J. (2010). Verification and Validation in Scientific Computing. *Cambridge University Press*, Cambridge.

Parkhurst, D. L., and Appelo, C. A. J. (2013). Description of input and examples for PHREEQC version 3—A computer program for speciation, batch-reaction, one-dimensional transport,

and inverse geochemical calculations: U.S. Geological Survey Techniques and Methods, book 6, chap. A43, 497 p., available only at http://pubs.usgs.gov/tm/06/a43/.

Peschard, I. (2010). Modeling and Experimenting. *P. Humphreys and C. Imbert (eds)*, *Models, Simulations, and Representations*, London: Routledge, 42–61.

Petitjean, A., Forquet, N., Wanko, A., Laurent, J., Molle, P., Mosé, R. and Sadowski, A. (2012). Modelling aerobic biodegradation in vertical flow sand filters: Impact of operational considerations on oxygen transfer and bacterial activity. *Water Research,* 46, 2270-2280.

Polyanin, A. D. (2002). Handbook of Linear Partial Differential Equations for Engineers and Scientists. Chapman & Hall/CRC Press, Boca Raton. ISBN 1-58-488-297-2.

Ribé, V., Nehrenheim, E., Odlare, M. and Waara, S. (2009). Leaching of contaminants from untreated pine bark in a batch study: Chemical analysis and ecotoxicological evaluation. *Journal of Hazardous Materials*, 163, 1096-1100.

Rizzo, A., Langergraber, G., Galvão, A., Boano, F., Revelli, R. and Ridolfi, L. (2014). Modelling the response of laboratory horizontal flow constructed wetlands to unsteady organic loads with HYDRUS-CWM1. *Ecological Engineering*, 68, 209-213.

Rohrlich, F. (1990). Computer Simulations in the Physical Sciences *Proceedings of the Biennial Meeting of the Philosophy of Science Association*, Published by: The University of Chicago Press on behalf of the Philosophy of Science Association, Chicago, 1990, 507-518.

Rudman, P., S. (2006). How Mathematics Happened: The First 50,000 Years. *Prometheus Books*, New York, ISBN 978-1-59102-477-4, 63.

Šimůnek, J., van Genuchten M., Th. and Šejna M. (2001). The HYDRUS Software Package for Simulating Two- and Three-Dimensional Movement of Water, Heat, and Multiple Solutes in Variably-Saturated Media. Technical Manual, Version 2.0 [Electronic]. PC Progress, Prague, Czech Republic, Available: http://www.pc-progress.com/en/Default.aspx?h3d-description (2015-02-24).

Scholz, M. and Xu, J. (2002). Performance comparision of experimental constructed wetlands with different filter media and macrophytes treating industrial wastewater contaminated with lead and copper. *Bioresource Technology*, 83, 71-79.

Subramani, T. and Akela, J. (2014). Onsite Waste Water Treatment System. *Journal of Engineering Research and Applications*, 4 (6), 154-162.

Tate, R. (1995). Soil Microbiology. *John Wiley & Sons*, New York, ISBN 0-471-57868-1.

Thompson, L. J., Gray, V., Lindsay, D. and von Holy, A. (2005). Carbon : nitrogen : phosphorus ratios influence biofolm formation by Enterobacter cloacae and Citrobacter freundii. *Journal of Applied Microbiology*, 101 (5), 1364-5072.

Tietz, A., Kirschner, A., Langergraber, G., Sleytr, K. and Haberl, R. (2007). Characterization of microbial biocoenosis in vertical subsurface flow constructed wetlands. *Science of total environment*, 380, 163-172.

Toscano, A., Langergraber, G., Consoli, S. and Cirelli, G., L. (2009). Modelling pollutant removal in a pilot-scale two-stage subsurface flow constructed wetlands. *Ecological Engineering*, 35, 281-289.

UN (United Nations), Department of Economic and Social Affairs, Population Division (2014).

USEPA (United States Environmental Protection Agency) (2002). Onsite wastewater treatment systems manual, Report EPA/625/R-00/008.

van Genuchten, M.Th. (1980). A closed-form equation for predicting the hydraulic conductivity of unsaturated soils. *Soil Science Society of America Journal* 44 (5), 892–898.

Vogel, T. and Císlerová M. (1988). On the reliability of unsaturated hydraulic conductivity calculated from the moisture retention curve, *Transport in Porous Media,* 3, 1-15.

World Urbanization Prospects: The 2014 Revision, Highlights (ST/ESA/SER.A/352).

Willmott, C. J. (1981). On the validation of models. *Physical Geography*, 2, 184–194.

Willmott, C. J., Ackleson, S. G., Davis, R. E., Feddema, J. J., Klink, K., M., Legates, D. R., O'Donnell, J., Rowe, C. M. (1985). Statistics for the evaluation of model performance. *Journal of Geophysical Research*, 90, 8995 – 9005.

Willmott, C. J., Robeson, S. M., Matsuura, K. (2012). Short communication A refined index of model performance. *International Journal of Climatology,* 32, 2088-2094.

WHO (World Health Organisation) (2006). WHO guidelines for the safe use of wastewater, excreta and greywater [Electronic]. Geneva: WHO. Available: http://www.who.int/water_sanitation_health/wastewater/gsuww/en/ (2015-02-23).

WWAP (World Water Assessment Programme) (2012). Managing Water under Uncertainty and Risk [Electronic]. Paris: UNESCO (The United Nations World Water Development Report 4). Available: *http://www.unesco.org/new/fileadmin/MULTIMEDIA/HQ/SC/pdf/WWDR4%20Volume%201-Managing%20Water%20under%20Uncertainty%20and%20Risk.pdf* (2015-02-23).

Xiuwen, Z., Fengmin, L., Lun, L., Mei, S. and Yuan, Y. (2014). The adsorption properties of ten CW substrates on phosphorus. *Environmental Engineering (CE)*, 40 (3), 49-52.

Acknowledgements

I want to give special thanks to my two main supervisors, Håkan Jönsson and for a short period Björn Vinnerås, who both gave me the best support they were capable of. I also want to thank my assistant supervisors, Sahar Dalahmeh, Mikael Pell and Günter Langergraber. Sahar Dalahmeh and Mikael Pell especially for their extensive commenting on manuscripts, which gave me a lot to think about and helped me improve my work greatly. Günter Langergraber was always early to give comments and was a great support for the HYDRUS wetland module challenges.

I thank Hans Liljenström who did a great job as my opponent at my pre-disp seminar. His comments helped me to improve the thesis greatly.

I thank all the members of the Environmental Engineering group: Agnes Willén, Allan Komakech, Annika Nordin, Cecilia Lalander, Jenna Senecal, Johanna Spångberg, Jørgen Fidjeland, Luis Fernando Perez Mercado, Petra Kohler, Stefan Diener, Sven Smårs and Yoon Lin Chiew.

I would like to thank the Head of the Department, Per-Anders Hansson, for the good advice he has given me (and all the signatures on various documents). I also thank Raida Jirjis, who gave me a lot of support during my doctoral studies and whom I admire for her great honesty. I am very grateful towards the always helpful and friendly administration team: Anna-Karin Johansson, Berit Wennberg, Jenny Björkegård, Maria Bywall and Marianne Lövgren.

Thanks to various un-named colleagues at SLU for friendly chats and interesting discussions about doing science and everything else.

Thanks to my friends outside SLU, I want to grow old together with everyone of you (Alicia, Lillbjäbb, Rasmus, Stina and Storbjäbb) so that we can keep on arguing all the way to Långvården (and beyond?). Thanks to my family, you truly made me what I am. Lastly, I want to thank Tomas, who carried me through this. *All my life I've waited for the sun to rise … And it's you*.

I am grateful for the funding provided by the Swedish Research Council Formas.

Appendix A

Appendix A contains an excerpt from the HYDRUS wetland module manual, p. 9-13, reproduced here with permission of the authors. The excerpt displays all equations and parameters of CW2D (the sub-setting of the HYDRUS wetland module).

3.4 CW2D biokinetic model

3.4.1 Stoichiometric matrix and reaction rates

Table 3.5 and Table 3.6 show stoichiometric coefficients for ammonium nitrogen and inorganic phosphorus, respectively. Table 3.7 shows the stoichiometric matrix of reactions in CW2D, whereas Table 3.8 shows the reaction rates.

Table 3.5: Stoichiometric coefficients for ammonium nitrogen.

$\nu_{1,N}$ =	$i_{N,CS} - (1 - f_{Hyd,CI}) \cdot i_{N,CR} - f_{Hyd,CI} \cdot i_{N,CI}$
$\nu_{2,N}$ =	$1/Y_H \cdot i_{N,CR} - i_{N,BM}$
$\nu_{3,N}$ =	$1/Y_H \cdot i_{N,CR} - i_{N,BM}$
$\nu_{4,N}$ =	$1/Y_H \cdot i_{N,CR} - i_{N,BM}$
$\nu_{5,N}$ =	$i_{N,BM} - (1 - f_{BM,CR} - f_{BM,CI}) \cdot i_{N,CS} - f_{BM,CR} \cdot i_{N,CR} - f_{BM,CI} \cdot i_{N,CI}$
$\nu_{6,N}$ =	$- 1/Y_{ANs} - i_{N,BM}$
$\nu_{7,N}$ =	$i_{N,BM} - (1 - f_{BM,CR} - f_{BM,CI}) \cdot i_{N,CS} - f_{BM,CR} \cdot i_{N,CR} - f_{BM,CI} \cdot i_{N,CI}$
$\nu_{8,N}$ =	$- i_{N,BM}$
$\nu_{9,N}$ =	$i_{N,BM} - (1 - f_{BM,CR} - f_{BM,CI}) \cdot i_{N,CS} - f_{BM,CR} \cdot i_{N,CR} - f_{BM,CI} \cdot i_{N,CI}$

See Table 3.10 for definitions of the composition and stoichiometric parameters.

Table 3.6: Stoichiometric coefficients for inorganic phosphorus.

$\nu_{1,P}$ =	$i_{P,CS} - (1 - f_{Hyd,CI}) \cdot i_{P,CR} - f_{Hyd,CI} \cdot i_{P,CI}$
$\nu_{2,P}$ =	$1/Y_H \cdot i_{P,CR} - i_{P,BM}$
$\nu_{3,P}$ =	$1/Y_H \cdot i_{P,CR} - i_{P,BM}$
$\nu_{4,P}$ =	$1/Y_H \cdot i_{P,CR} - i_{P,BM}$
$\nu_{5,P}$ =	$i_{P,BM} - (1 - f_{BM,CR} - f_{BM,CI}) \cdot i_{P,CS} - f_{BM,CR} \cdot i_{P,CR} - f_{BM,CI} \cdot i_{P,CI}$
$\nu_{6,P}$ =	$- i_{P,BM}$
$\nu_{7,P}$ =	$i_{P,BM} - (1 - f_{BM,CR} - f_{BM,CI}) \cdot i_{P,CS} - f_{BM,CR} \cdot i_{P,CR} - f_{BM,CI} \cdot i_{P,CI}$
$\nu_{8,P}$ =	$- i_{P,BM}$
$\nu_{9,P}$ =	$i_{P,BM} - (1 - f_{BM,CR} - f_{BM,CI}) \cdot i_{P,CS} - f_{BM,CR} \cdot i_{P,CR} - f_{BM,CI} \cdot i_{P,CI}$

See Table 3.10 for definitions of the composition and stoichiometric parameters.

Table 3.7: Stoichiometric matrix of reactions in CW2D (Langergraber and Šimůnek, 2005; see Table 3.10 for definitions of the stoichiometric coefficients).

R	№ Components:	1 O2	2 CR	3 CS	4 CI	5 XH	6 XANs	7 XANb	8 NH4N	9 NO2N	10 NO3N	11 N2N	12 IP
		gO2	gCOD						gN				gP
			Heterotrophic organisms										
1	Hydrolysis			−1	f_{INCI}				v_{1N}				v_{1P}
2	Aerobic growth of heterotrophs on readily biodegradable COD	$1 - 1/Y_H$	$1 - f_{INCR}$ $-1/Y_H$			1			v_{2N}				v_{2P}
3	Nitrate-based growth of heterotrophs on readily biodegradable COD		$-1/Y_H$			1			v_{3N}		$-(1 - Y_H)/2.86Y_H$	$(1 - Y_H)/2.86Y_H$	v_{3P}
4	Nitrite-based growth of heterotrophs on readily biodegradable COD		$-1/Y_H$			1			v_{4N}	$-(1 - Y_H)/1.71Y_H$		$(1 - Y_H)/1.71Y_H$	v_{4P}
5	Lysis of heterotrophs		f_{INCR}	$1 - f_{INCR} - f_{INCI}$	f_{INCI}	−1			v_{5N}				v_{5P}
			Autotrophic organisms 1—*Nitrosomonas*										
6	Aerobic growth of *Nitrosomonas* on ammonium	$-(3.43 - Y_{AN})/Y_{AN}$					1		$i_{N,BM}$	$-1/Y_{AN}$	$1/Y_{AN}$		v_{6P}
7	Lysis of *Nitrosomonas*		f_{INCR}	$1 - f_{INCR} - f_{INCI}$	f_{INCI}		−1		v_{7N}				v_{7P}
			Autotrophic organisms 2—*Nitrobacter*										
8	Aerobic growth of *Nitrobacter* on nitrite	$-(1.14 - Y_{AN})/Y_{AN}$						1	v_{8N}	$-1/Y_{AN}$	$1/Y_{AN}$		v_{8P}
9	Lysis of *Nitrobacter*		f_{INCR}	$1 - f_{INCR} - f_{INCI}$	f_{INCI}			−1	v_{9N}				v_{9P}

Table 3.8: Reaction rates in CW2D (Langergraber and Šimůnek, 2005).

R	Process / Reaction rate rc_j
Heterotrophic organisms	
1	Hydrolysis $K_h \cdot \frac{c_{CS}/c_{XH}}{K_X + c_{CS}/c_{XH}} \cdot c_{XH}$
2	Aerobic growth of heterotrophs on readily biodegradable COD $\mu_H \cdot \frac{c_{O2}}{K_{Het,O2} + c_{O2}} \cdot \frac{c_{CR}}{K_{Het,CR} + c_{CR}} \cdot f_{N,Het} \cdot c_{XH}$
3	NO3-growth of heterotrophs on readily biodegradable COD $\mu_{DN} \cdot \frac{K_{DN,O2}}{K_{DN,O2} + c_{O2}} \cdot \frac{c_{NO3}}{K_{DN,NO3} + c_{NO3}} \cdot \frac{K_{DN,NO2}}{K_{DN,NO2} + c_{NO2}} \cdot \frac{c_{CR}}{K_{DN,CR} + c_{CR}} \cdot f_{N,DN} \cdot c_{XH}$
4	NO2-growth of heterotrophs on readily biodegradable COD $\mu_{DN} \cdot \frac{K_{DN,O2}}{K_{DN,O2} + c_{O2}} \cdot \frac{c_{NO2}}{K_{DN,NO2} + c_{NO2}} \cdot \frac{c_{CR}}{K_{DN,CR} + c_{CR}} \cdot f_{N,DN} \cdot c_{XH}$
5	Lysis of heterotrophs $b_H \cdot c_{XH}$
Autotrophic organisms 1 – *Nitrosomonas*	
6	Aerobic growth of *Nitrosomonas* on NH4 $\mu_{ANs} \cdot \frac{c_{O2}}{K_{ANs,O2} + c_{O2}} \cdot \frac{c_{NH4}}{K_{ANs,NH4} + c_{NH4}} \cdot \frac{c_{IP}}{K_{ANs,IP} + c_{IP}} \cdot c_{XANs}$
7	Lysis of *Nitrosomonas* $b_{HANs} \cdot c_{XANs}$
Autotrophic organisms 2 – *Nitrobacter*	
8	Aerobic growth of *Nitrobacter* on NO2 $\mu_{ANb} \cdot \frac{c_{O2}}{K_{ANb,O2} + c_{O2}} \cdot \frac{c_{NO2}}{K_{ANb,NO2} + c_{NO2}} \cdot f_{N,ANb} \cdot c_{XANb}$
9	Lysis of *Nitrobacter* $b_{HANb} \cdot c_{XANb}$
Conversion of solid and liquid phase concentrations	
	$c_{XY} = \frac{\rho}{\theta} \cdot s_{XY}$, where $Y = H, ANs, ANb$
Factor for nutrients	
	$f_{N,x} = \frac{c_{NH4}}{K_{x,NH4} + c_{NH4}} \cdot \frac{c_{IP}}{K_{x,IP} + c_{IP}}$, where $x = Het, DN, ANb$

See Table 3.9 for definitions of rate coefficients.

3.4.2 Model parameters

Table 3.9 shows the kinetic parameters, and Table 3.10 the temperature dependences, stoichiometric parameters, composition parameters and parameters describing oxygen transfer for the CW2D biokinetic model as described in Langergraber and Šimůnek (2005).

Table 3.9: Kinetic parameters in the CW2D biokinetic model (Langergraber and Šimůnek, 2005).

	Description [unit]	Value
Hydrolysis		for 20°C (10°C)
K_h	hydrolysis rate constant [1/d]	3 (2)
K_X	saturation/inhibition coefficient for hydrolysis [g COD_{CS}/g COD_{BM}]	0.1 (0.22) *
Heterotrophic bacteria (aerobic growth)		
μ_H	maximum aerobic growth rate on CR [1/d]	6 (3)
b_H	rate constant for lysis [1/d]	0.4 (0.2)
$K_{het,O2}$	saturation/inhibition coefficient for S_O [mg O_2/L]	0.2
$K_{het,CR}$	saturation/inhibition coefficient for substrate [mg COD_{CR}/L]	2
$K_{het,NH4N}$	saturation/inhibition coefficient for NH4 (nutrient) [mg N/L]	0.05
$K_{het,IP}$	saturation/inhibition coefficient for P [mg N/L]	0.01
Heterotrophic bacteria (denitrification)		
μ_{DN}	maximum aerobic growth rate on CR [1/d]	4.8 (2.4)
$K_{DN,O2}$	saturation/inhibition coefficient for S_O [mg O_2/L]	0.2
$K_{DN,NO3N}$	saturation/inhibition coefficient for NO3 [mg N/L]	0.5
$K_{DN,NO2N}$	saturation/inhibition coefficient for NO2 [mg N/L]	0.5
$K_{DN,CR}$	saturation/inhibition coefficient for substrate [mg COD_{CR}/L]	4
$K_{DN,NH4N}$	saturation/inhibition coefficient for NH4 (nutrient) [mg N/L]	0.05
$K_{DN,IP}$	saturation/inhibition coefficient for P [mg N/L]	0.01
Ammonia oxidising bacteria (*Nitrosomonas* spp.)		
μ_{ANs}	maximum aerobic growth rate on S_{NH} [1/d]	0.9 (0.3)
b_{ANs}	rate constant for lysis [1/d]	0.15 (0.05)
$K_{ANs,O2}$	saturation/inhibition coefficient for S_O [mg O_2/L]	1
$K_{ANs,NH4N}$	saturation/inhibition coefficient for NH4 [mg N/L]	0.5
$K_{ANs,IP}$	saturation/inhibition coefficient for P [mg N/L]	0.01
Nitrite oxidising bacteria (*Nitrobacter* spp.)		
μ_{ANb}	maximum aerobic growth rate on S_{NH} [1/d]	1 (0.35)
b_{ANb}	rate constant for lysis [1/d]	0.15 (0.05) *
$K_{ANb,O2}$	saturation/inhibition coefficient for S_O [mg O_2/L]	0.1
$K_{ANb,NO2N}$	saturation/inhibition coefficient for NO2 [mg N/L]	0.1
$K_{ANb,NH4N}$	saturation/inhibition coefficient for NH4 (nutrient) [mg N/L]	0.05
$K_{ANb,IP}$	saturation/inhibition coefficient for P [mg N/L]	0.01

* Langergraber (2007)

Table 3.10: Temperature dependences, stoichiometric parameters, composition parameters and parameters describing oxygen transfer in the CW2D biokinetic model (Langergraber and Šimůnek, 2005).

Parameter	Description [unit]	Value
Temperature dependences (activation energy [J/mol] for Arrhenius equation**)**		
Tdep_het	Activation energy for processes caused by XH [J/mol]	47800
Tdep_aut	Activation energy for processes caused by XA [J/mol]	69000
Tdep_Kh	Activation energy Hydrolyses [J/mol]	28000
Tdep_KX	Activation energy factor KX for hydrolyses [J/mol]	-53000 *
Tdep_KNHA	Activation energy for factor KNHA for nitrification [J/mol]	-160000 *
Stoichiometric parameters		
$f_{Hyd,CI}$	production of CI in hydrolysis	0.0
$f_{BM,CR}$	fraction of CR generated in biomass lysis	0.1
$f_{BM,CI}$	fraction of CI generated in biomass lysis	0.02
Y_{Het}	yield coefficient for XH	0.63
Y_{ANs}	yield coefficient for XANs	0.24
Y_{ANb}	yield coefficient for XANb	0.24
Composition parameters		
$i_{N,CR}$	N content of CR [g N/g COD_{CR}]	0.03
$i_{N,CS}$	N content of CS [g N/g COD_{CS}]	0.04
$i_{N,CI}$	N content of CI [g N/g COD_{CI}]	0.01
$i_{N,BM}$	N content of biomass [g N/g COD_{BM}]	0.07
$i_{P,CR}$	P content of CR [g P/g COD_{CR}]	0.01
$i_{P,CS}$	P content of CS [g P/g COD_{CS}]	0.01
$i_{P,CI}$	P content of CI [g P/g COD_{CI}]	0.01
$i_{P,BM}$	P content of biomass [g P/g COD_{BM}]	0.02
Oxygen		
cO2_sat_20	saturation concentration of oxygen [g/m³]	9.18
Tdep_cO2_sat	activation energy for saturation concentration of oxygen [J/mol]	-15000
rate_O2	re-aeration rate [1/d]	240

* Langergraber (2007)

Appendix B

Table B1. *Bark filter model sensitivity analysis. For abbreviations, see Appendix A*

	Effluent COD % change					
Factor times the base-scenario parameter value	0.5	0.8	0.9	1.1	1.2	1.5
α	122	-1	-1	0	1	3
$K_{Anb,IP}$	0	0	0	0	0	0
$K_{Anb,NH4N}$	0	0	0	0	0	0
$K_{Anb,NO2N}$	0	0	0	0	0	0
$K_{Anb,O2}$	0	0	0	0	0	0
$K_{Ans,IP}$	0	0	0	0	0	0
$K_{Ans,NH4N}$	0	0	0	0	0	0
$K_{ANs,O2}$	0	0	0	0	0	0
$K_{DN,CR}$	0	0	0	0	0	0
$K_{DN,IP}$	0	0	0	0	0	0
$K_{DN,NH4N}$	0	0	0	0	0	0
$K_{DN,NO2N}$	0	0	0	0	0	0
$K_{DN,NO3N}$	0	0	0	0	0	0
$K_{DN,O2}$	0	0	0	0	0	0
$K_{het,CR}$	3	1	0	0	-1	-2
$K_{het,IP}$	1	0	0	0	0	-1
$K_{het,NH4N}$	0	0	0	0	0	0
$K_{het,O2}$	2	0	0	0	0	-1
K_X	-4	-2	-1	1	2	4
K_h	23	3	1	-1	-2	-3
K_s	1	2	0	1	0	-1
Tdep_KNHA	0	0	0	0	0	0
Tdep_KX	0	0	0	0	0	0
Tdep_Kh	0	0	0	0	0	0
Tdep_aut	0	0	0	0	0	0
Tdep_het	0	0	0	0	0	0
Y_{ANb}	0	0	0	0	0	0
Y_{ANs}	0	0	0	0	0	0
Y_{Het}	-3	-3	-1	2	4	24
b_{ANb}	0	0	0	0	0	0
b_{ANs}	0	0	0	0	0	0
b_H	-23	-9	-4	4	8	20
$f_{BM,CI}$	-20	-8	-4	4	8	20
$f_{BM,CR}$	1	0	0	0	0	-1
$f_{Hyd,CI}$	0	0	0	0	0	0

$i_{N,BM}$	0	0	0	0	0	0
$i_{N,CI}$	0	0	0	0	0	0
$i_{N,CR}$	0	0	0	0	0	0
$i_{N,CS}$	0	0	0	0	0	0
$i_{P,BM}$	0	0	0	0	0	1
$i_{P,CI}$	0	0	0	0	0	0
$i_{P,CR}$	0	0	0	0	0	0
$i_{P,CS}$	0	0	0	0	0	0
l	-1	0	0	0	0	0
μ_{ANb}	0	0	0	0	0	0
μ_{ANs}	0	0	0	0	0	0
μ_{DN}	0	0	0	0	0	0
μ_H	-5	-2	-1	1	2	3
n	5	2	4	-1	-12	-
θ_r	-7	-3	0	0	3	4
θ_s	24	1	1	0	0	-1

Table B2. *Charcoal filter model sensitivity analysis. For abbreviations, see Appendix A*

	Effluent COD % change					
Factor times the base-scenario parameter value	0.5	0.8	0.9	1.1	1.2	1.5
α	-3	-1	-1	0	1	2
$K_{Anb,IP}$	0	0	0	0	0	0
$K_{Anb,NH4N}$	0	0	0	0	0	0
$K_{Anb,NO2N}$	0	0	0	0	0	0
$K_{Anb,O2}$	0	0	0	0	0	0
$K_{Ans,IP}$	0	0	0	0	0	0
$K_{Ans,NH4N}$	0	0	0	0	0	0
$K_{ANs,O2}$	0	0	0	0	0	0
$K_{DN,CR}$	0	0	0	0	0	0
$K_{DN,IP}$	0	0	0	0	0	0
$K_{DN,NH4N}$	0	0	0	0	0	0
$K_{DN,NO2N}$	0	0	0	0	0	0
$K_{DN,NO3N}$	0	0	0	0	0	0
$K_{DN,O2}$	0	0	0	0	0	0
$K_{het,CR}$	0	0	0	0	0	1
$K_{het,IP}$	-2	-1	0	0	0	1
$K_{het,NH4N}$	0	0	0	0	0	0
$K_{het,O2}$	-1	-1	0	0	0	1
K_X	-9	-4	-2	2	4	11
K_h	71	8	3	-2	-4	-7
K_s	-	0	0	0	0	0
Tdep_KNHA	0	0	0	0	0	0
Tdep_KX	0	0	0	0	0	0
Tdep_Kh	0	0	0	0	0	0
Tdep_aut	0	0	0	0	0	0
Tdep_het	0	0	0	0	0	0
Y_{ANb}	0	0	0	0	0	0
Y_{ANs}	0	0	0	0	0	0
Y_{Het}	-36	-19	-11	12	104	1121
b_{ANb}	0	0	0	0	0	0
b_{ANs}	0	0	0	0	0	0
b_H	-22	-8	-4	3	6	13
$f_{BM,CI}$	-20	-8	-4	4	8	20
$f_{BM,CR}$	1	1	0	0	-1	-1
$f_{Hyd,CI}$	0	0	0	0	0	0
$i_{N,BM}$	15	0	0	0	0	0

$i_{N,CI}$	0	0	0	0	0	0
$i_{N,CR}$	0	0	0	0	0	8
$i_{N,CS}$	0	0	0	0	0	0
$i_{P,BM}$	-4	-1	0	0	1	0
$i_{P,CI}$	0	0	0	0	0	0
$i_{P,CR}$	0	0	0	0	0	0
$i_{P,CS}$	0	0	0	0	0	0
l	0	0	0	0	0	0
μ_{ANb}	0	0	0	0	0	0
μ_{ANs}	0	0	0	0	0	0
μ_{DN}	0	0	0	0	0	0
μ_{H}	4	1	1	-1	-1	-2
n	-	-	-3	3	6	13
θ_r	8	2	1	-1	-2	11
θ_s	484	8	3	-3	-6	-9

Table B3. *Sand filter model sensitivity analysis. For abbreviations, see Appendix A*

	Effluent COD % change					
Factor times the base-scenario parameter value	0.5	0.8	0.9	1.1	1.2	1.5
α inner	-58	-17	-9	1	5	9
α wall layer	-61	-16	-8	-3	-7	-33
$K_{Anb,IP}$	0	0	0	0	0	0
$K_{Anb,NH4N}$	-1	0	0	0	0	0
$K_{Anb,NO2N}$	-2	-1	0	0	0	0
$K_{Anb,O2}$	0	0	0	0	0	0
$K_{Ans,IP}$	-1	0	0	0	0	0
$K_{Ans,NH4N}$	0	0	0	0	0	0
$K_{ANs,O2}$	0	0	0	0	0	0
$K_{DN,CR}$	1	0	0	0	0	-1
$K_{DN,IP}$	0	0	0	0	0	0
$K_{DN,NH4N}$	0	0	0	0	0	0
$K_{DN,NO2N}$	0	0	0	0	0	0
$K_{DN,NO3N}$	0	0	0	0	0	0
$K_{DN,O2}$	-1	-1	0	0	0	0
$K_{het,CR}$	2	-1	0	0	0	1
$K_{het,IP}$	-1	0	0	0	0	0
$K_{het,NH4N}$	0	-1	0	0	0	1
$K_{het,O2}$	-6	-2	-1	1	2	4
K_X	-3	-2	-1	1	1	3
K_h	9	2	1	-1	-2	-3
K_s *inner*	-3	0	-2	-2	-1	-2
K_s *wall layer*	-15	-5	-3	-2	0	4
Tdep_KNHA	0	0	0	0	0	0
Tdep_KX	0	0	0	0	0	0
Tdep_Kh	0	0	0	0	0	0
Tdep_aut	0	0	0	0	0	0
Tdep_het	0	0	0	0	0	0
Y_{ANb}	-5	-1	0	0	0	0
Y_{ANs}	-1	-1	0	0	0	0
Y_{Het}	-12	0	0	0	4	48
b_{ANb}	0	0	0	0	0	0
b_{ANs}	0	0	0	0	0	0
b_H	-6	-3	-2	1	3	9
$f_{BM,CI}$	-2	-1	-1	0	0	1
$f_{BM,CR}$	0	0	0	0	0	-1

$f_{Hyd,CI}$	0	0	0	0	0	0
$i_{N,BM}$	23	0	0	0	0	3
$i_{N,CI}$	-1	0	0	0	0	0
$i_{N,CR}$	4	1	0	-1	-1	4
$i_{N,CS}$	5	2	1	-1	-2	-4
$i_{P,BM}$	-2	-1	-1	0	0	1
$i_{P,CI}$	0	0	0	0	0	0
$i_{P,CR}$	0	0	0	0	-1	-1
$i_{P,CS}$	0	0	0	0	0	-1
l inner	3	0	-2	-1	-3	-6
l wall layer	0	1	-1	-4	-4	-8
μ_{ANb}	1	0	0	-1	-1	-2
μ_{ANs}	2	0	0	0	0	-1
μ_{DN}	5	2	1	-1	-2	-5
μ_{H}	13	3	1	-2	-3	-3
n inner	-35	-15	-9	2	5	7
n wall layer	-44	-6	-5	-11	-8	-
θ_r *inner*	6	1	-1	-4	-8	-11
θ_r *wall layer*	-1	0	0	-1	-2	-1
θ_s *inner*	34	13	3	-8	-17	-31
θ_s *wall layer*	14	9	6	-12	-20	-47